UCRL 9595

UNIVERSITY OF CALIFORNIA

Ernest O. Lawrence Radiation Laboratory

INVESTIGATION OF NUCLEAR REACTIONS BY RECOIL STUDIES OF RADIOACTIVE PRODUCTS

TWO-WEEK LOAN COPY

This is a Library Circulating Copy which may be borrowed for two weeks. For a personal retention copy, call Tech. Info. Division, Ext. 5545

DISCLAIMER

This document was prepared as an account of work sponsored by the United States Government. While this document is believed to contain correct information, neither the United States Government nor any agency thereof, nor the Regents of the University of California, nor any of their employees, makes any warranty, express or implied, or assumes any legal responsibility for the accuracy, completeness, or usefulness of any information, apparatus, product, or process disclosed, or represents that its use would not infringe privately owned rights. Reference herein to any specific commercial product, process, or service by its trade name, trademark, manufacturer, or otherwise, does not necessarily constitute or imply its endorsement, recommendation, or favoring by the United States Government or any agency thereof, or the Regents of the University of California. The views and opinions of authors expressed herein do not necessarily state or reflect those of the United States Government or any agency thereof or the Regents of the University of California.

UCRL-9595
UC-4 Chemistry General
TID-4500 (16th Ed.)

UNIVERSITY OF CALIFORNIA
Lawrence Radiation Laboratory
Berkeley, California

Contract No. W-7405-eng-48

INVESTIGATION OF NUCLEAR REACTIONS BY RECOIL STUDIES OF RADIOACTIVE PRODUCTS

John R. Morton III

(Thesis)

April, 1961

Printed in USA. Price $2.25. Available from the
Office of Technical Services
U. S. Department of Commerce
Washington 25, D.C.

INVESTIGATION OF NUCLEAR REACTIONS BY RECOIL STUDIES OF RADIOACTIVE PRODUCTS

Contents

Abstract 4

I. Introduction 5

II. Experimental Procedures

A. Angular Distribution Studies

1. Preparation of targets 7

2. Bombardment procedures 8

3. Counting procedures for reactions producing alpha-radioactive products 10

4. Counting procedures for reactions producing gamma-emitting radioactive products 14

5. Treatment of data 16

B. Range Studies

1. Preparation of targets 18

2. Bombardment procedures 18

3. Counting procedures for reactions producing alpha-radioactive products 21

4. Counting procedures for reactions producing gamma-emitting radioactive products 24

5. Treatment of data 26

III. Monte Carlo Calculations 27

A. The Isotropic Case 27

B. The Nonisotropic Case 35

C. Discussion of the Monte Carlo Calculations

1. Anisotropy 43

2. Nuclear Temperature 43

3. Excitation Not Removed by Neutron Emission: E_γ . . . 44

4. Effect of Angular Resolution 44

IV. Results 45

A. $Ra^{226}(\alpha, 4n)Th^{226}$ 47

B. $Pb^{208}(\alpha, 2n)Po^{210}$ 54

Contents (continued)

C. $Pb^{207}(\alpha, n)Po^{210}$ 54
D. $Te^{130}(C^{12}, 5n)Ce^{137m}$ 54
E. $Pr^{141}(C^{12}, 4n)Tb^{149}$ 54

V. Discussion

A. Reactions that Can Be Fitted by the Calculations
1. $Pr^{141}(C^{12}, 4n)Tb^{149}$ 70
2. $Ra^{226}(\alpha, 4n)Th^{226}$ 70

B. Reactions that Can Not Be Fitted by the Simple Calculations
1. $Te^{130}(C^{12}, 5n)Ce^{137m}$ 71
2. $Pb^{208}(\alpha, 2n)Po^{210}$ 74
3. $Pb^{207}(\alpha, n)Po^{210}$ 76

VI. Concluding Remarks 78

Acknowledgments 79

Appendices

A. Program listing for the isotropic Monte Carlo calculation 80

B. Program listing for the nonisotropic Monte Carlo calculation 85

C. Program listings for the subroutines written for the Monte Carlo calculations 92

D. Derivations of the integral probability functions used in the calculations 97

E. Summary of calculated recoil angular distributions 98

References 106

INVESTIGATION OF NUCLEAR REACTIONS BY RECOIL STUDIES OF RADIOACTIVE PRODUCTS

John R. Morton III

(Thesis)

Department of Chemistry and Lawrence Radiation Laboratory
University of California
Berkeley, California

April, 1961

ABSTRACT

The ranges and angular distributions of the recoiling residual nuclei from several nuclear reactions have been studied to obtain information about the reaction mechanisms. The observed reactions were $Ra^{226}(\alpha, 4n)Th^{226}$, $Pb^{208}(\alpha, 2n)Po^{210}$, $Pr^{141}(C^{12}, 4n)Tb^{149}$, $Te^{130}(C^{12}, 5n)Ce^{137m}$, and $Pb^{207}(\alpha, n)Po^{210}$. The experimental angular distributions were compared with distributions calculated by a Monte Carlo method based upon the compound-nucleus and statistical models. The results from the $Ra^{226}(\alpha, 4n)$ and $Pr^{141}(C^{12}, 4n)$ reactions are in agreement with the simple theory. The $Te^{130}(C^{12}, 5n)$ data can be explained by formation of a compound nucleus which de-excites with enhanced probability for gamma emission. The $Pb^{208}(\alpha, 2n)$ and $Pb^{207}(\alpha, n)$ experiments require substantial contributions from direct-interaction mechanisms.

I. INTRODUCTION

Studies of nuclear reactions have been most commonly made by either of two general techniques: (a) The energy and angular spectra of the emitted light particles having been examined, total cross sections for producing the particles are then determined by integrating over the entire solid angle; and (b) The cross sections for formation of specific radioactive products have been determined by radiochemical techniques. In this case, the particular reaction leading to a given product can usually be determined from the conditions of the experiment; the total reaction cross section can be determined by summing the cross sections for all possible products.

When the chief interest is in the reaction mode leading to one particular product, the energy and angular distributions of the emitted light products may not give adequate information, even though in principle such an approach should be most informative. Complicating factors might be the production of light particles by several competing mechanisms, the double-valued energy spectrum for emitted light particles, and, where neutrons are emitted, the usual difficulties in obtaining precise neutron measurements. Because of these difficulties, the techniques of (b) have usually been favored, and much study of nuclear reaction mechanisms has been made in this way.

It has recently been recognized that additional useful information about the details of nuclear reactions can be obtained from study of the ranges and angular distributions of the recoiling product nuclei.[1-3] Recoil techniques have been found particularly useful for study of reactions involving emission of several neutrons.

Donovan and co-workers applied recoil techniques to the study of the reactions $Bi^{209}(\alpha, xn)$, $Bi^{209}(d, xn)$ and $Cm^{244}(\alpha, 2n)$.[1, 2] These workers also developed a Monte Carlo method for calculating the angular distributions of the recoiling product nuclei resulting from isotropic evaporation from the compound nucleus. Certain of the reactions in their study seemed consistent with this mechanism, while others did not.

The work presented here was undertaken to examine further the details of the Monte Carlo method, and to test the model with additional reactions.

The reactions selected for this study were $Ra^{226}(\alpha, 4n)Th^{226}$, $Pb^{208}(\alpha, 2n)Po^{210}$, $Pr^{141}(C^{12}, 4n)Tb^{149}$, $Pb^{207}(\alpha, n)Po^{210}$, and $Te^{130}(C^{12}, 5n)Ce^{137m}$. These reactions were selected because good cross-section data are available, and because they involve nuclei both near and distant from closed nuclear shells, in that part of the heavy-element region where fission is relatively improbable. To simplify the interpretation of counting data, reactions were selected whenever possible that produced alpha radioactive products. The reaction with Te^{130} was chosen because of some unusual features noted by Choppin and co-workers in the study of the excitation functions.[4, 5] Ranges and angular distributions were measured for the recoiling residual nuclei in each case except $Pb^{207}(\alpha, n)$, for which only the recoil angular distributions were measured.

II. EXPERIMENTAL PROCEDURES

A. Angular Distribution Studies

1. Preparation of Targets

a. Ra^{226} targets. The Ra^{226} targets were prepared by vacuum vaporization of radium chloride onto 0.001-in. aluminum foil. A drop of $RaCl_2$ solution was evaporated to dryness on a tantalum ribbon electrically heated to redness inside a bell jar. The system was evacuated and the ribbon was briefly heated to white heat, vaporizing the radium salt onto the foil suspended above. Thickness of the radium deposit was controlled by the length of the heating period, and was determined by direct alpha count of a known area of the aluminum foil in a low-geometry (0.12%) alpha scintillation counter. Thickness of the radium on the foil was found to be $1.2 \pm 0.2\ \mu g/cm^2$.

b. Pb^{208} targets. The composition of the enriched isotope used was Pb^{208}, $96.0 \pm 0.1\%$; Pb^{207}, $2.8 \pm 0.1\%$; Pb^{206}, $1.2 \pm 0.1\%$; and Pb^{204}, $< 0.1\%$.[6] The targets were prepared by vacuum evaporation of lead metal from a graphite crucible onto 0.001-in. aluminum foil. Target thickness was determined by chemically analyzing a known area of the foil for lead content, using the dithizone method.[7] This procedure involved extraction of the lead from aqueous solution by dithizone; the absorption of the colored complex was then measured in a spectrophotometer at 510 mμ. The lead concentration was determined by comparison with a calibration curve prepared from known standards. A blank determination was made with a sample of the aluminum foil. The thickness of the lead deposit was found to be $1.0 \pm 0.2\ \mu g/cm^2$.

c. Pb^{207} targets. The composition of the enriched isotope used was Pb^{207}, $71.5 \pm 0.2\%$; Pb^{208}, $25 \pm 0.2\%$; Pb^{206}, $3.5 \pm 0.1\%$; and Pb^{204}, $< 0.2\%$.[6] These targets were prepared in the same way as the Pb^{208} targets. The thickness of the deposit in this case was $0.50 \pm 0.08\ \mu g/cm^2$.

d. Te^{130} targets. These targets were prepared by electroplating enriched Te^{130} onto gold foils 10^{-4} in. thick. The technique is a modification of the procedure described by Choppin.[5] The gold foils were cleaned, dried, and weighed. These foils, supported on a piece of soft rubber backing, served as the cathode of a standard glass plating cell. The foil was sealed to the cell with label varnish. The electrolyte was

3 cc of 3 M perchloric acid containing 0.2 mg/ml of Te^{130}. The anode was positioned approximately 0.5 cm above the cathode. A current of 0.4 to 0.5 ma, at 1.8 to 1.9 v, was allowed to flow for about 5 minutes. The uniformity of the plate was observed through the sides of the cell. If the deposit began to plate unevenly, polarity was reversed until the tellurium was cleanly removed, and the plating process was repeated. The cell was disassembled by removing the varnish with alternate washes of water and acetone. Finally the foils were dried and weighed. The thickness of the plated deposit was determined by the difference in the foil weights before and after plating. The targets used in these experiments ranged from 10 to 30 $\mu g/cm^2$. The error in target thickness was about ± 5 $\mu g/cm^2$. Plating yields attainable by this procedure were about 30%.

e. Pr^{141} targets. The praseodymium targets were prepared by vacuum evaporation of Pr metal onto 0.00025-in. aluminum foils. The thickness of the deposit was determined by the difference in weights of the foils before and after coating. The targets used in these experiments contained 24.6 ± 5.0 $\mu g/cm^2$ Pr^{141}.

2. Bombardment Procedures

The helium-ion (alpha particle) bombardments were done at the Crocker Radiation Laboratory 60-inch cyclotron. The carbon-ion bombardments were done at the heavy-ion linear accelerator (Hilac).

The particle-beam energies were adjusted through use of aluminum degrading foils. The range-energy data of Aron and co-workers were used in adjusting the energies of the helium-ion beam.[8] The carbon-ion beam energy was adjusted according to the range-energy data of Walton[9], which are also consistent with the published data of Northcliffe.[10]

The recoil target assembly used in all experiments is shown schematically in Fig. 1. The supporting foil for the targets was mounted so that the surface containing the target material faced away from the particle beam. A circular catcher foil, 0.001-in. aluminum foil 4.6 cm in diameter, was placed directly behind the target and centered on the beam axis. The target-to-catcher spacing was adjusted to intercept the desired maximum angle of recoil; for these bombardments this distance

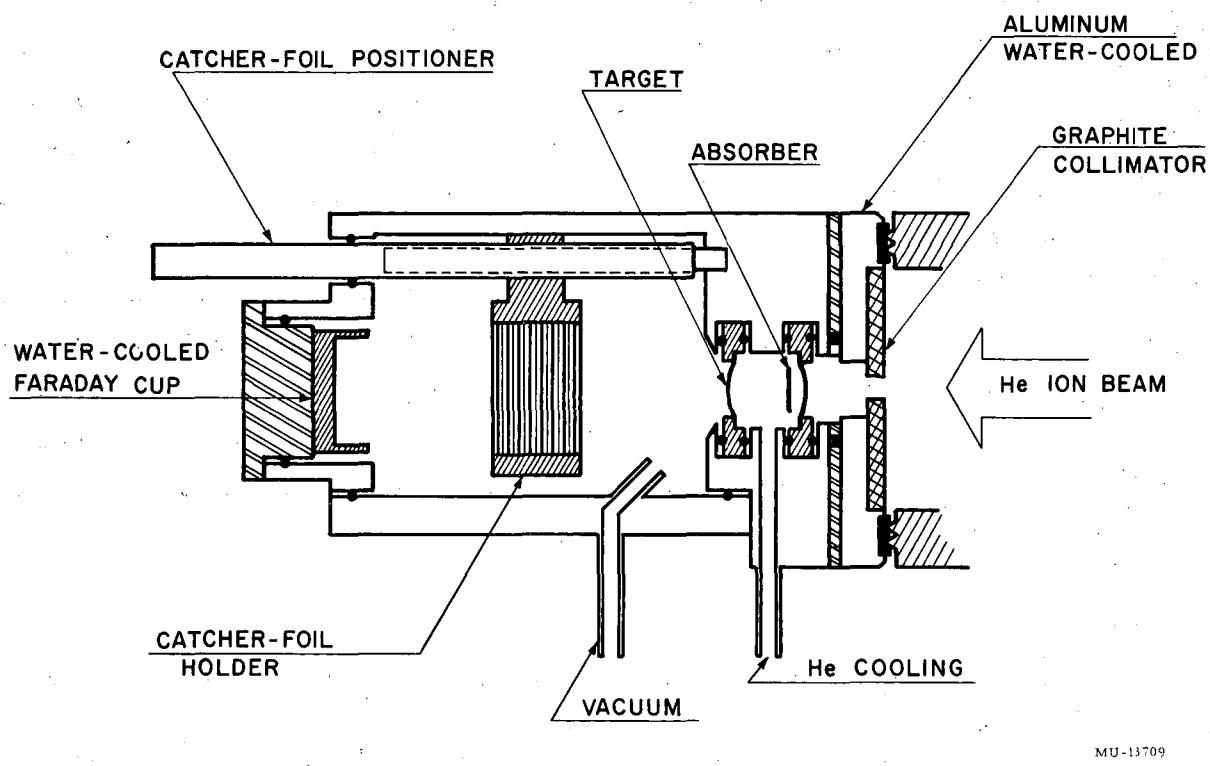

Fig. 1. Recoil target assembly

was either 4.0 or 6.0 cm, corresponding respectively to maximum angles with the beam axis of 29.8 and 20.9 degrees. The chamber at the rear of the target foil was evacuated to a pressure of approx. 10^{-3} mm of mercury.

The position of the particle beam was fixed by using a graphite collimator with a 1/8-in. circular aperture. The target foil was cooled during the bombardment by circulating helium gas over the surface facing the beam. After passing through the aluminum catcher foil, the beam was collected in an air-cooled Faraday cup electrically insulated from the other parts of the assembly. The beam current was measured with a beam-integrating electrometer. Maximum beam currents for these experiments were 0.4 μamp for helium-ion bombardments and 0.2 to 0.4 μamp for the carbon-ion bombardments, assuming fully stripped ions. These limits depended upon the target material being used; they were imposed to prevent evaporation of the target material from the backing foil due to the heating effect of high beam currents.

At the end of the bombardment the catcher foil was removed and cut into eleven concentric rings by a die cutter in a hydraulic press at 5000 psi.

3. Counting Procedures for Reactions Producing Alpha-Radioactive Products

Each ring was counted for total alpha activity. When necessary for identification of products, mixtures of alpha activities were resolved by use of an alpha-particle pulse-height analyzer.

The following specific techniques were used to identify and count the products of the reactions listed.

a. $Ra^{226}(\alpha, 4n)Th^{226}$; Q = - 29.44 Mev.[11] At helium ion energies greater than about 37 Mev, pulse-height analysis and gross alpha-decay counts showed that substantially all the alpha-emitting products were Th^{226} (30.9 min)[12] and its short-lived decay daughters Ra^{222} (38 sec)[12], Rn^{218} (0.019 sec)[12], and Po^{214} (1.6×10^{-4} sec).[13] This is shown in Fig. 2. This mixture decayed effectively with the half life of Th^{226}; therefore, at these energies a gross alpha count was sufficient for measuring the relative yields of Th^{226}.

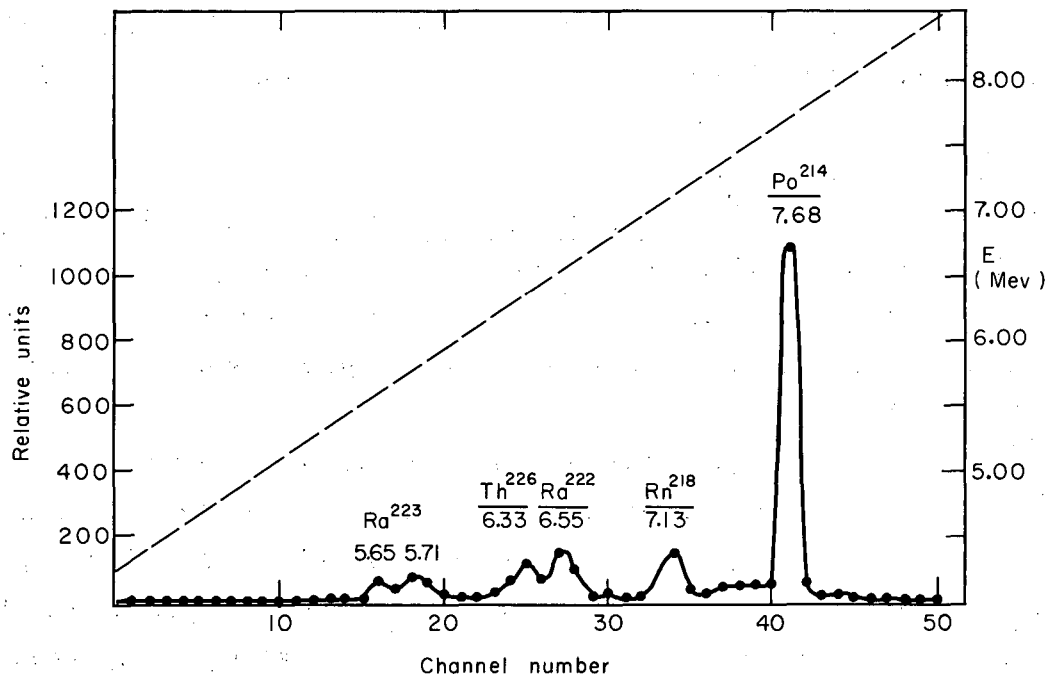

MU-23025

Fig. 2. Pulse-height analysis of Ring 2, $\theta = 5.97$ deg (solid line) and energy vs channel number (dashed line) for products of the reaction $Ra^{226}(\alpha, 4n)Th^{226}$ at 38.2 Mev bombarding energy. The activities with symbols underscored are decay products of Th^{226}.

It is also possible to obtain some Po^{214} from the decay of Rn^{222} (3.8 d)[14] and its daughters from the radium target itself.[15] This possibility was minimized by heating the target for about 30 min under an infrared lamp prior to bombardment; the heating removed the emanations in equilibrium with the radium on the target surface.

At helium-ion energies less than about 37 Mev, yields of the (α, 3n) product (Th^{227}) and its decay series became significant. It then became necessary to resolve the Th^{226} products on the alpha pulse-height analyzer.

b. $Pb^{208}(\alpha, 2n)Po^{210}$; Q = - 19.52 Mev.[11] Pulse-height analysis and gross alpha decay counts indicated that the only significant product of this reaction was Po^{210} (138.4 d)[16]; consequently, only gross alpha counts of each ring were required. Figure 3 shows a typical pulse-height analysis.

In these bombardments, 5 to 15% of the total Po^{210} activity observed in the center ring of the catcher was due to activation of trace impurities of lead in the catcher foil itself. This impurity effect was measured by bombarding a blank "target" foil and catcher foil under normal experimental conditions at an energy corresponding to the highest cross section for this reaction. Assuming the primary impurity to be Pb^{208}, all the gross activities in the first ring for the various experiments were reduced by this impurity content in proportion to the cross section at the particular bombarding energy and the total particle flux received. This procedure was checked further by counting both the front and back sides of the first ring and taking the recoil Po^{210} activity to be the difference between the two counts, and was based upon the assumption that the induced activities should be uniformly distributed throughout the volume of the foil, whereas the recoil activity should be near the surface facing the target. The corrections calculated by these two methods agreed very closely. Correction was negligible for the second ring.

c. $Pb^{207}(\alpha, n)Po^{210}$; Q = - 12.15 Mev.[11] Alpha pulse-height analysis showed Po^{210} to be the only significant alpha-emitting product; therefore, gross alpha counting was also suitable for these experiments.

Because of the 25% isotopic impurity of Pb^{208} in these targets, the yield of Po^{210} from the $Pb^{208}(\alpha, 2n)$ reaction was substantial for

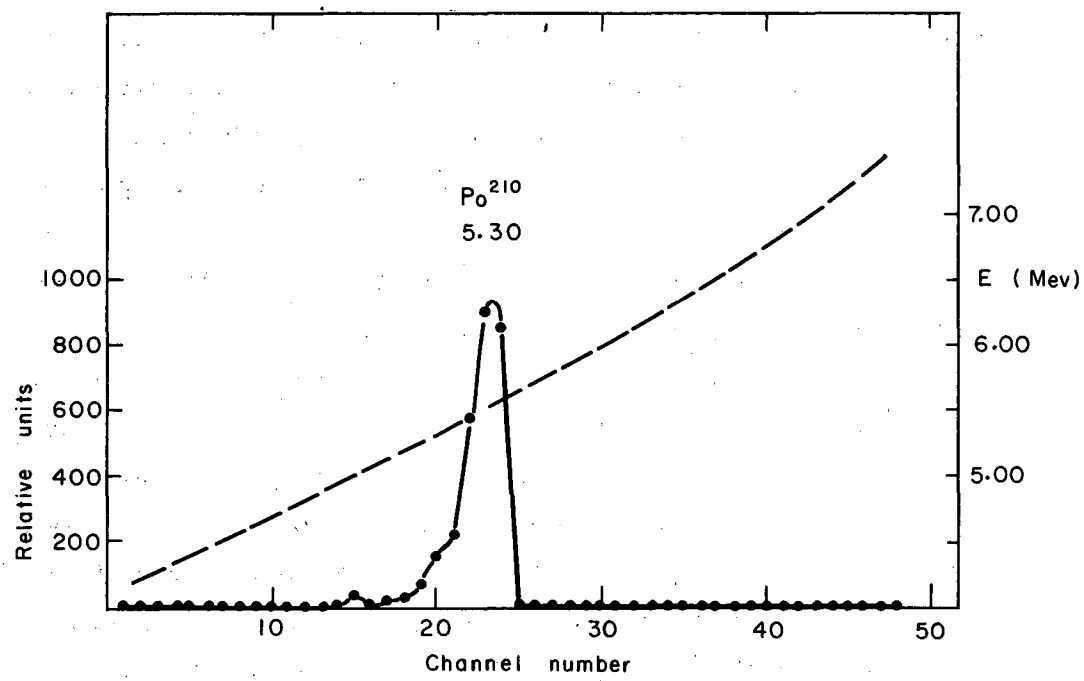

MU-23026

Fig. 3. Pulse-height analysis of Ring 3, $\theta = 8.71$ deg (solid line) and energy vs channel number (dashed line) for products of the reaction $Pb^{208}(\alpha, 2n)Po^{210}$ at 31.7 Mev bombarding energy.

practically every bombardment.[17] This contribution was corrected in the following way: The amount of Pb^{208} in the Pb^{207} targets was precisely determined by measuring the yield of Po^{210} produced at 29.7 Mev, which is near the maximum $Pb^{208}(\alpha, 2n)$ cross section. At that energy the total yield of Po^{210} comes from Pb^{208}; the $Pb^{207}(\alpha, 2n)$ product, Po^{209} (103 yr)[18], was not produced in sufficient quantity to interfere. The experimental recoil angular distributions for the $Pb^{207}(\alpha, n)$ reaction were then corrected by subtracting, point for point, the $Pb^{208}(\alpha, 2n)$ angular distributions taken at corresponding bombarding energies; these $Pb^{208}(\alpha, 2n)$ angular distributions had been adjusted in yield corresponding to the Pb^{208} content of the Pb^{207} targets and the conditions of the particular experiment.

d. $Pr^{141}(C^{12}, 4n)Tb^{149}$; Q = - 44.9 Mev.[19] Alpha pulse-height analysis and gross alpha-decay counts showed the major alpha-emitting product to be Tb^{149} (4.1 hr)[20]. Figure 4 shows a typical pulse-height analysis. When the catcher foils were counted soon after the end of the bombardments at energies greater than about 65 Mev, 10% to 20% of the activity in the innermost ring was due to some unidentified short-lived product. After about 4 hr, the short-lived component decayed away; then the gross decay followed the characteristic half-life of Tb^{149}. This short-lived activity may have been produced from some impurity in the catcher foil.

4. Counting Procedures for Reactions Producing Gamma-Emitting Radioactive Products

$Te^{130}(C^{12}, 5n)Ce^{137m}$; Q = - 40.8 Mev.[21] For this system, the probable yield of numerous beta- and gamma-emitting products made it necessary to separate the cerium activity radiochemically from the other products before counting. The separation was accomplished by the standard procedure for removal of cerium by carrier-precipitation as the oxalate[23]. The chemical yields were initially determined by weighing the vacuum-dried precipitates on weighed glass-fiber filter pads. This was checked later by repeating the separation in the same way and then igniting the oxalate to the oxide for final weighing. Agreement between the two sets of results was excellent. The filter cakes were then mounted for counting as

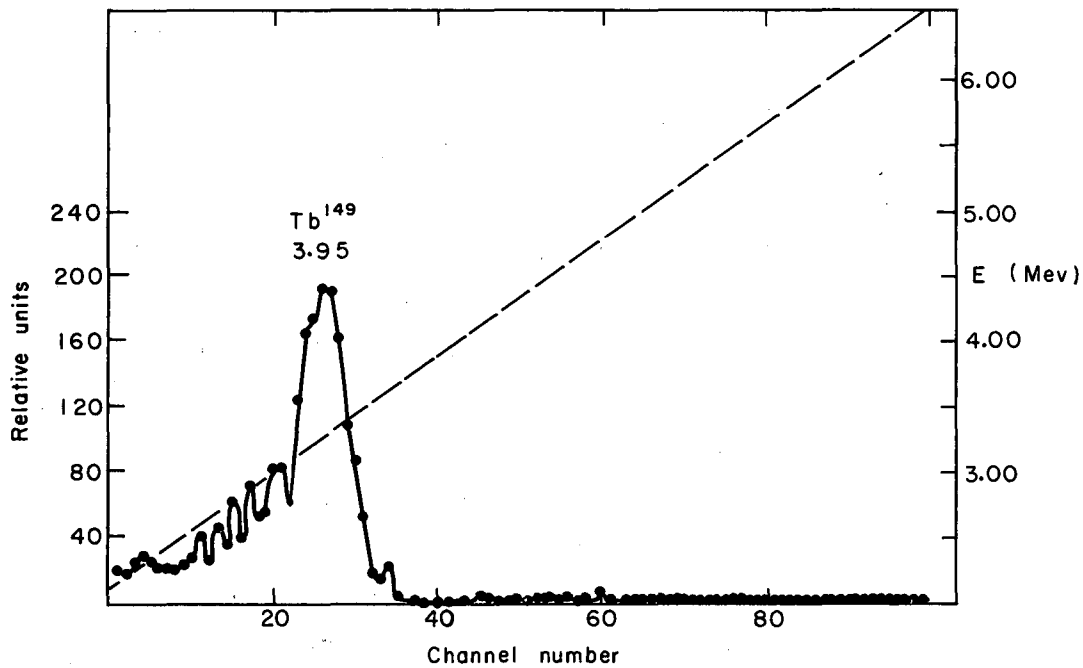

MU-23027

Fig. 4. Pulse-height analysis of Ring 2, $\theta = 3.99$ deg (solid line) and energy vs channel number (dashed line) for products of the reaction $Pr^{141}(C^{12}, 4n)Tb^{149}$ at 61.5 Mev bombarding energy.

described by Bayhurst and Prestwood[24] and Blann.[25] The relative content of Ce^{137m} (34.5 hr)[26] was conveniently determined by counting the 230-kev conversion electrons[27] from the 255-kev isomeric transition.[26] The mass assignment for this activity has been checked several times.[26, 28, 29] Decays of the samples were followed for 5 to 7 days. The decay curve for the Ce^{137m} was resolved graphically in each case.

5. Treatment of Data

For each experiment, the product activity in each ring was determined. Where necessary, corrections were applied for decay before and during the counting period. Corrections for contaminating activities were made as previously described.

The cerium data were corrected for chemical yield; self-absorption corrections were applied, based upon the data in Ref. 24 for 232-kev conversion electrons from Ba^{135m}.

The activities in each ring were corrected for solid angle. Then plots were prepared of the logarithm of the relative differential cross section as a function of the angle of the recoil with respect to the beam axis, in the laboratory system.

In the $Pb^{208}(\alpha, 2n)$ experiments, a correction in the bombarding energy due to beam-particle energy straggling in the degrading foils was considered; however, the correction was only about 0.1 Mev beginning at about 33 Mev.[30] This is within the limit of uncertainty in the beam energy. Definitive information is not currently available for carbon-ion beam energy straggling.

For the $Ra^{226}(\alpha, 4n)$ and $Pb^{208}(\alpha, 2n)$ reactions, a trial-and-error correction was made for scattering of the beam particles in the foils, using a graphical method of adding together the experimentally determined beam-scatter distributions,[31] and a recoil angular distribution of arbitrary shape, to obtain the experimental angular distribution. This correction was about 0.5 deg at the angle for which the differential cross section was reduced to half its forward value; however, it was much more significant at larger angles. This correction was not attempted in the carbon-ion bombardments. Unlike those with He^4 ions, these experiments showed practically no recoil events beyond

the maximum calculated angle of deflection of the recoiling nucleus; consequently, any correction for beam spread would be expected to be smaller than that for the He^4 cases, and well within the limits of experimental error at the half-value angle.

B. RANGE STUDIES

1. Preparation of Targets

a. Natural tellurium targets. Natural tellurium was used for this purpose because of the requirement for thicker target deposits supported on aluminum. The targets were prepared by vacuum evaporation of natural tellurium metal[32] from a hot tantalum strip onto 0.00025-in. aluminum foil. The thickness of the target layer was determined by weighing the foils before and after the evaporation. The targets used in these experiments contained 240 $\mu g/cm^2$ of tellurium.

b. Natural lead targets. Natural lead was used for this purpose for the same reason as given above. The targets were prepared by vacuum evaporation of natural lead metal,[33] by the same technique as for the Pb^{208} targets. The yield in this case was calculated by assuming complete evaporation of a measured quantity of lead metal through a solid angle fixed by the shape of the graphite crucible. The resulting target thickness was 5.6 ± 0.5 mg/cm^2.

2. Bombardment Procedures

The recoil range studies described here were of two general types: (a) The thick-target integral-range experiment of the type described in Refs. 3 and 34. In this type of experiment the target used is much thicker than the average range of the recoiling product nuclei. The target support foil is positioned so that the coated surface faces away from the beam; behind the target a catcher foil is positioned. The ratio of the average projected recoil range to the target surface density is given by the relation

$$\frac{\text{Average range}}{\text{Target surface density}} = \frac{\text{Recoil activity in catcher foil}}{\text{Recoil activity in both target and catcher foil}} .$$

(b) The thin-target differential-range experiment requires a target relatively thin with respect to the average range of the recoils. The recoils travel through a degrading medium until they are stopped; then the number of recoils at various ranges is determined. The activities are distributed about the average projected range in the medium.

The specific procedures used for study of each reaction are described below.

a. $Ra^{226}(\alpha, 4n)Th^{226}$. The experimental assembly and targets used for the recoil angular distributions were also used for these experiments. An insulated electrode was installed inside the recoil chamber below and parallel to the beam axis. A gas make-up system was connected to allow the chamber to be evacuated and filled with hydrogen at low pressure. Target cooling, collimation, beam monitoring, and beam-energy adjustment were as previously described. Details of the modified assembly are shown in Fig. 5. Before bombardment, an 8.2-cm-long strip of aluminum sheet, marked at 2-mm intervals, was attached to the top of the insulated electrode. The chamber was evacuated and flushed with hydrogen to eliminate traces of air; then the hydrogen pressure was adjusted to 2.4 to 4.0 cm of mercury. This range of pressure placed the average range of the recoils approximately half-way down the length of the strip. The electrode and catcher strips were set at a potential 600 v negative with respect to the other parts of the assembly. Collection efficiencies of recoils with this technique ranged from 65% to 85%. At the end of the bombardment the catcher foil was removed and divided into 2-mm sections for counting.

b. Natural Pb + He^4. This experiment used the thick-target method already mentioned. The recoil-target assembly was also used. A foil stack was prepared from 15 of the natural lead targets, with coated surfaces facing away from the beam, each followed by a 0.001-in. aluminum catcher foil. The stack was mounted in the evacuated recoil chamber of the assembly and bombarded with the full-energy alpha-particle beam. This arrangement permitted simultaneous bombardment of targets in an energy range from 15 to 47 Mev. The target stack was not cooled, so it was necessary to maintain the beam current at about 0.05 μamp to avoid damage to the lead coatings. Since the stack of foils was thick enough to stop the beam particles, the beam was measured by connecting the beam-integrating electrometer directly to the targets.

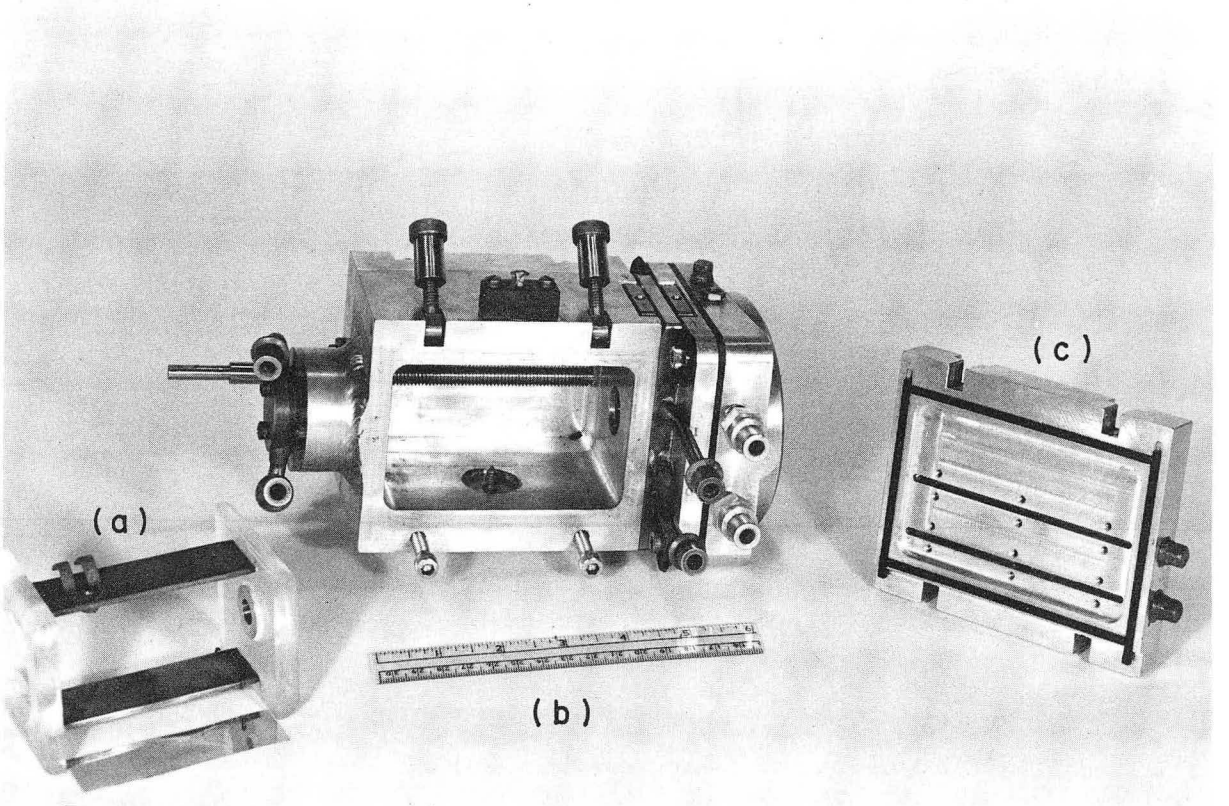

ZN-2746

Fig. 5. Recoil target assembly modified for range measurements of Th^{226} recoil atoms. From left to right: (a) parallel-plate insert for target chamber — aluminum collector strip lying in front; (b) target assembly with recoil chamber open; (c) cover to recoil chamber.

c. Natural Te + C^{12}. These experiments used the differential range technique; the stopping medium was a stack of aluminum leaf. The aluminum foils used had surface densities of 164 and 169 $\mu g/cm^2$. Extensive studies of foil homogeneity were not made. The arrangement was: the target foil, mounted with coated side facing away from the beam, followed by six pieces of aluminum leaf and one piece of 0.0005-in. aluminum foil. Four such stacks were mounted in tandem in a Hilac copper water-cooled target holder.[25] This arrangement permitted the ranges to be measured at four different energies simultaneously.

3. Counting Procedures for Reactions Producing Alpha-Radioactive Products

The specific counting procedures are discussed separately for the individual reactions studied.

a. $Ra^{226}(\alpha, 4n)Th^{226}$. The sections of the catcher strip were counted for total alpha activities and, when necessary, mixtures of alpha activities were resolved by use of the alpha pulse-height analyzer. The counting problems have already been described in Sec. II-A-3(a) above.

b. Natural Pb + He^4. After 2 weeks' decay, each target and catcher foil was counted for gross alpha activities. After 30 days' decay the gross count was rechecked, and the catcher foils were counted on the alpha pulse-height analyzer. There was essentially no difference between the two gross alpha counts; this is consistent with the absence of short-lived alpha activities. The alpha pulse-height analysis indicated the products to be Po products from $Pb(\alpha, xn)$ reactions. A typical pulse-height analysis is shown in Fig. 6. The products observed in significant quantities were Po^{208} and Po^{210}. Table I shows that this is not surprising. Another possible source of Po^{210} was the 10^{-4}% bismuth impurity in the lead target material. The $Bi^{209}(\alpha, 3n)At^{210}$ reaction product decays to Po^{210} by K-electron capture;[35] the total Po^{210} produced by this mechanism should have contributed less than 1 α count per minute (< 0.7%) at the most favorable energy for the $(\alpha, 3n)$ reactions. Any amounts of At^{209} (5.5 hr)[36] and At^{211} (7.2 hr)[37] produced would have completely decayed before the alpha counting was done.

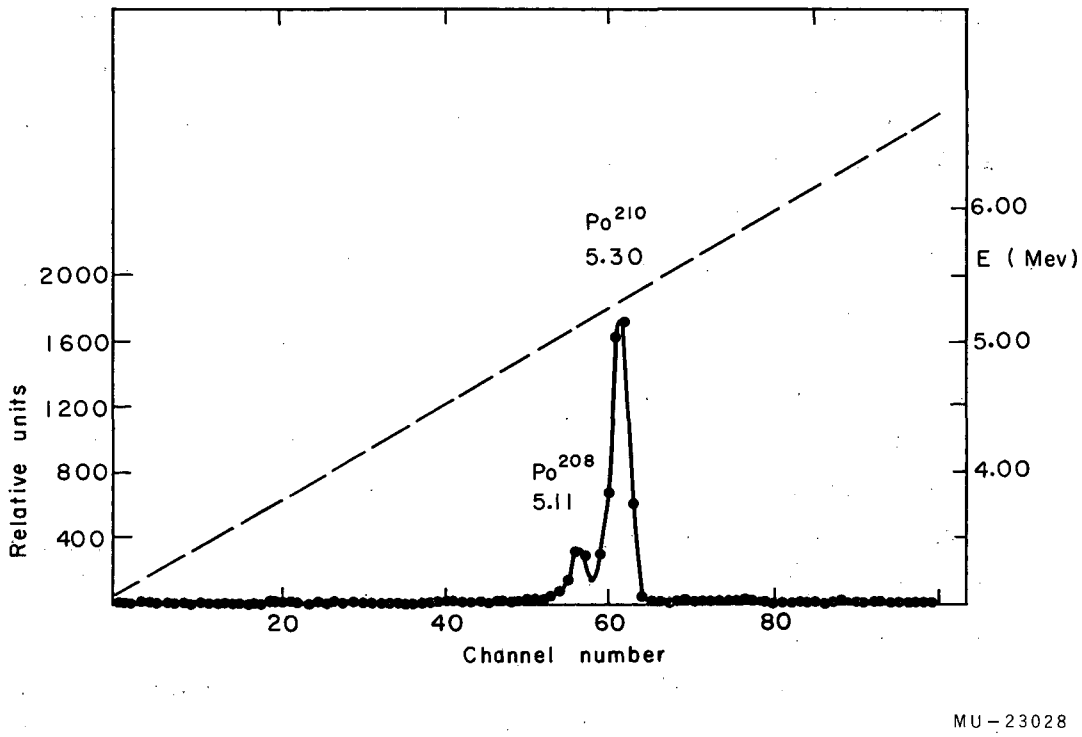

Fig. 6. Alpha pulse-height analysis of the catcher foil containing the gross recoil products from the reactions of natural Pb+He^4 at 30.1 Mev. Broken line is a plot of energy vs channel number.

Table I. Products from natural Pb + He^4

	Pb^{204}	Pb^{206}	Pb^{207}	Pb^{208}
Abundance	(1.4%)	(25.1%)	(21.7%)	(52.3%)
Reaction:				
(α, n)	Po^{207}(5.7h, α, EC)	Po^{209}(103y, α)	Po^{210}(138d, α)	Po^{211}(25s, α)
(α, 2n)	Po^{206}(8.8d, α, EC)	Po^{208}(2.93y, α)	Po^{209}(103y, α)	Po^{210}(138d, α)
(α, 3n)	Po^{205}(1.8h, α, EC)	Po^{207}(5.7h, α, EC)	Po^{208}(2.93y, α)	Po^{209}(103y, α)
(α, 4n)	Po^{204}(3.8h, α, EC)	Po^{206}(8.8d, α, EC)	Po^{207}(5.7h, α, EC)	Po^{208}(2.93y, α)

4. Counting Procedures for Reactions Producing Gamma-Emitting Radioactive Products

Natural Te + C^{12}. In order to count these reaction products it was necessary to separate them chemically from the aluminum foils. Because of the large number of foils used in a given bombardment, the chemical procedure[23] was abbreviated somewhat by eliminating the steps for removing the lanthanum activities, otherwise the treatment was as described in Sec. II-A-4 above. The resulting samples represented the combined cerium and lanthanum products, that is, the products of both the (C^{12}, xn) and (C^{12}, pxn) reactions.

The bombarding energies for these experiments were 70, 80.3, 90, and 99.5 Mev. From Choppin's excitation functions,[4] only the (C^{12}, 4n-6n) reactions would be expected. Presumably the (C^{12}, p3n-p5n) reactions would also occur. The products of these reactions for the three most abundant tellurium isotopes are listed in Table II, together with their radioactive properties.

Decays of the activities were followed for 7 days. Graphs of the decay data were prepared. In this case it was not possible to clearly identify most of the specific products. The decay curves could be generally resolved into a long-lived group with half-life ranges of 46 to 92 hr and a short-lived group with half-lives ranging from 8 to 13 hr. Reference to Table II shows that we might expect to see three groups of activities in this period of counting: a group with half-lives of about 4 to 6 hours, a second with half-lives of about 19 to 40 hours, and a third with the 72-hr half-life due to the electron-capture decay product of Ce^{134}. The very short-lived and very long-lived products should not be observed. The decay data are consistent with this reasoning, although it is not possible to cleanly resolve a mixture of so many activities with half-lives so nearly equal.

Table II. Products from natural Te + C^{12}

	Te^{126}	Te^{128}	Te^{130}
Abundances	(18.7%)	(31.8%)	(34.5%)
Reactions:			
(C^{12}, 4n)	Ce^{134}(72hr, E.C.) La^{134}(6.5min, β^+) Ba^{134}(stable)	Ce^{136}(stable)	Ce^{138}(stable)
(C^{12}, 5n)	Ce^{133}(6.3hr, β^+) La^{133}(4hr, β^+) Ba^{133m}(38.8hr, I.T.)	Ce^{135}(22hr, β^+) La^{135}(19.5hr, E.C.) Ba^{135m}(28.7hr, E.C.)	Ce^{137m}(34.5hr, I.T.) La^{137}($6x10^4$yr, E.C.)
(C^{12}, 6n)	Ce^{132}(4.2hr, β^+) La^{132}(4.5hr, β^+) Ba^{132}(stable)	Ce^{134}(72hr, E.C.) La^{134}(6.5min, β^+) Ba^{134}(stable)	Ce^{136}(stable)
(C^{12}, p3n)	La^{134}(6.5min, β^+) Ba^{134}(stable)	La^{136}(9.5min, β^+) Ba^{136}(stable)	La^{138}(10^{11}yr, β^-)
(C^{12}, p4n)	La^{133}(4hr, β^+) Ba^{133m}(38.8hr, I.T.)	La^{135}(19.5hr, E.C.) Ba^{135m}(28.7hr, I.T.)	La^{137}($6x10^4$yr, E.C.)
(C^{12}, p5n)	La^{132}(4.5hr, β^+) Ba^{132}(stable)	La^{134}(6.5min, β^+) Ba^{134}(stable)	La^{136}(9.5min, β^+) Ba^{136}(stable)

5. Treatment of Data

a. $Ra^{226}(\alpha, 4n)Th^{226}$. The data were corrected for decay before and during the counting period. They were also corrected for differences in areas of the sections of catcher strips by normalizing to a unit size, determined by weighing. Probability plots were constructed from the recoil data, from which were determined the mean ranges and the range straggling.

b. Natural Pb + He^4. From the product yields in the targets and catchers the mean range was calculated for each target. A plot was then constructed of recoil range vs bombarding energy.

c. Natural Te + C^{12}. The data were corrected for chemical yield and self-absorption. The range was corrected for the thickness of targets. Probability plots were constructed for both long- and short-lived activities, and the mean ranges and the range straggling determined from these.

III. MONTE CARLO CALCULATIONS

The application of Monte Carlo methods to nuclear reaction studies was originally suggested by Ulam and von Neumann.[38] The technique was initially used by Goldberger for a nuclear cascade model.[39] Qualitative success has been reported by a number of other authors in treatments of nuclear cascade processes.[40-52] Meadows[44], Jackson,[53] and Rudstam[47] have used the Monte Carlo approach to discuss experimental cross sections in terms of the evaporation model. Dostrovsky and collaborators have made very elaborate Monte Carlo calculations in treatment of various details of nuclear evaporation processes such as fission-spallation competition,[54] cross sections,[52,55] and energy spectra of the particles emitted.[52,55,56]

The Monte Carlo technique was originally applied to the calculation of the angular distribution of the recoiling residual nuclei from nuclear reactions to permit a comparison of experimental recoil-angular distributions with the compound-nucleus and statistical models. The Monte Carlo calculation described below for the case of isotropic neutron evaporation is essentially that developed by Donovan;[1] it has been reprogrammed for use with the IBM 704 computer.

The calculation is based upon the "evaporation" of neutrons from a compound nucleus formed by amalgamation of the projectile particle into the target nucleus.[57-59]

A. The Isotropic Case

A number of simplifying assumptions were incorporated in the calculation:

(a) De-excitation of the compound nucleus proceeds solely by neutron emission as long as the available excitation energy exceeds the binding energy of the last neutron.

(b) The energy spectrum of the evaporated neutrons has the form, following Jackson[60]

$$P(E_n)\, dE_n = E_n e^{-E_n/T}\, dE_n, \qquad (3.1)$$

where $P(E_n)$ is the probability of emitting a neutron of energy between E_n and $E_n + dE_n$. T is a parameter commonly called the "nuclear temperature." Application of this form of spectrum has been discussed by Donovan and co-workers.[1]

(c) The neutrons are evaporated isotropically in the system of the recoiling nucleus.

(d) The parameter T is assumed to be constant throughout the evaporation sequence. The value for T used in each case was selected by trial and error, by the procedure devised by Jackson[60] to obtain the best detailed fit to the experimental excitation function for the reaction of interest. The "temperature" obtained in this way can be considered to have the significance of an average temperature (expressed in terms of kT) of the residual nucleus during the entire evaporation cascade. Figure 7 shows that the calculation is relatively insensitive to variations in T of a few tenths Mev, and becomes increasingly insensitive for larger numbers of neutrons evaporated.

(e) The recoiling nucleus is considered to move a negligible distance in the laboratory system while the neutrons are evaporating during the $\ll 10^{-15}$-sec lifetime of the compound nucleus.[57]

(f) The mass of the recoiling nucleus is unchanged during the evaporation process. This assumption gives an error of about 2% for the reaction $Te^{130}(C^{12}, 5n)Ce^{137}$; the error is greatly reduced for heavier elements and fewer neutrons evaporated.

(g) The momenta of the recoiling nuclei are unchanged by the change in mass as the neutrons evaporate. The error in the angle of recoil for the $Te^{130}(C^{12}, 5n)Ce^{137}$ reaction is about 2.5%, and is correspondingly reduced for heavier target nuclei.

(h) The maximum excitation energy available as kinetic energy to the neutrons is given by $E_{pcm} + Q_n - E_\gamma$, where E_{pcm} is the energy of the projectile particle in the center-of-mass system, Q_n is the Q for the reaction in which n neutrons are emitted, and E_γ represents some portion of the excitation energy not available as kinetic energy for the neutrons. The shape of the calculated recoil angular distributions is fairly sensitive to the value of E_γ used. The degree of this sensitivity is shown in Fig. 8.

The neutron energies were randomly selected to fit the chosen form of spectrum by use of the following procedure:

An integral probability function was derived by integration of (1) (see Appendix D-1) to give

$$Z(N) = e^{-E_n/T} \left(\frac{E_n}{T} + 1 \right) , \qquad (3.2)$$

which is shown graphically in Fig. 9.

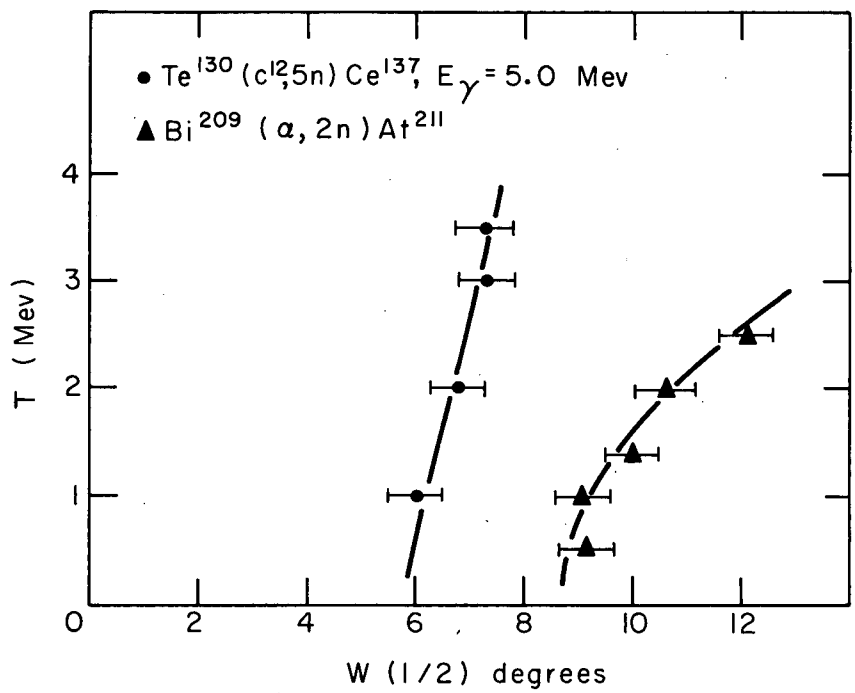

MU-23029

Fig. 7. Plot of the magnitude of the angle W(1/2) at which the relative differential cross section is reduced to half the forward value as a function of nuclear temperature.

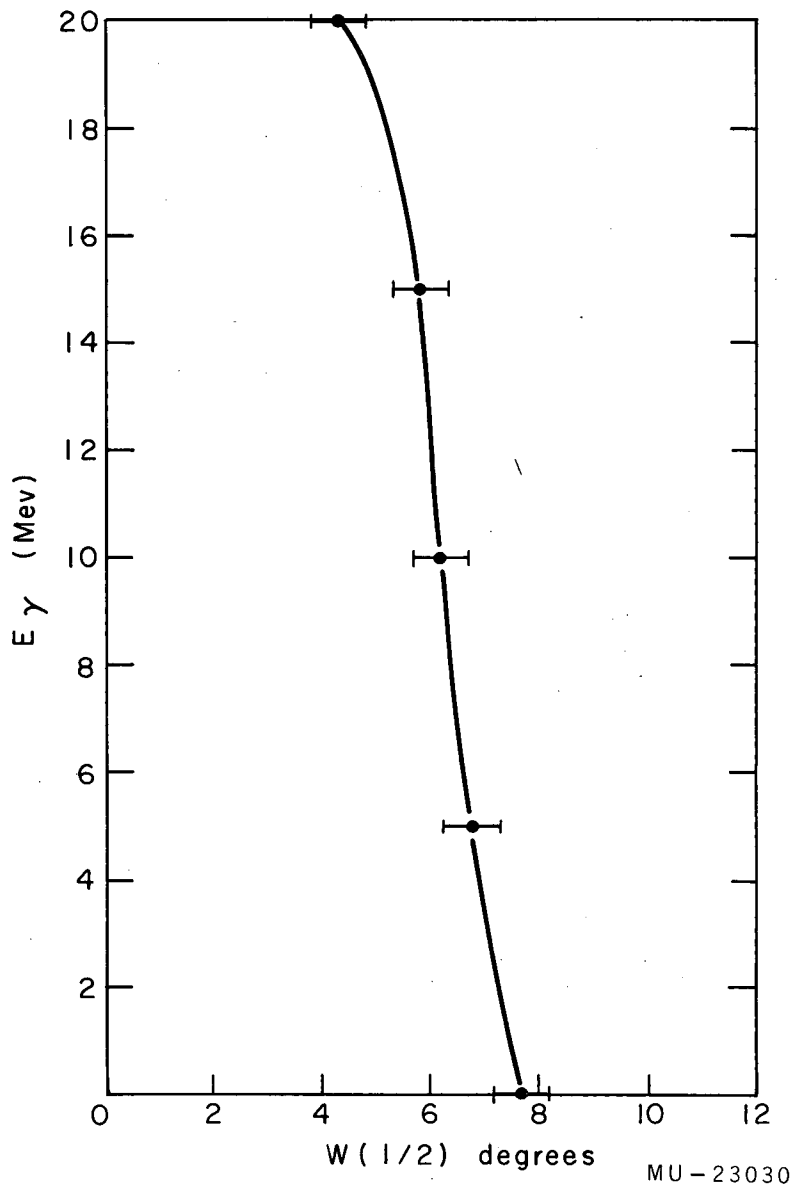

Fig. 8. Plot of the magnitude of the angle W(1/2) at which the relative differential cross section is reduced to half the forward value as a function of E_γ for the reaction $Te^{130}(C^{12}, 5n)Ce^{137}$. $E_{C^{12}}$ = 75 Mev, T = 2.5 Mev.

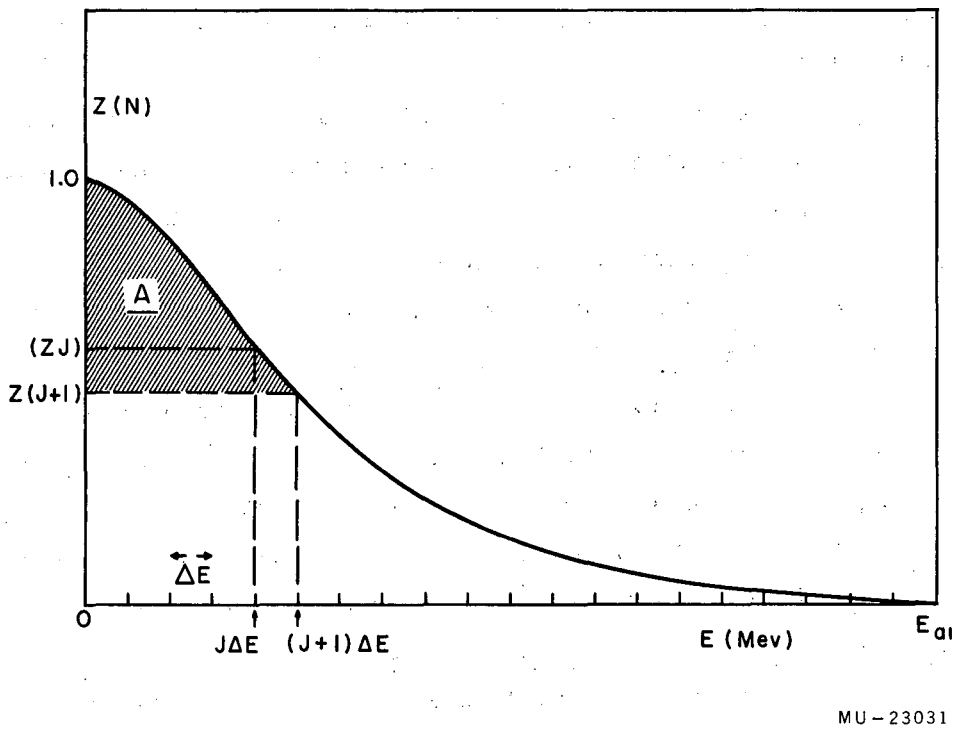

Fig. 9. Integral probability function for neutron energy selection. Scales are greatly exaggerated.

Because of difficulty in solving for a unique value of E_n from a given randomly chosen value for Z(N), a 2049-space table of $Z[(n-1)\,\Delta E]$ was used in the computation, where ΔE is defined by

$$\Delta E = \frac{E_{pcm} + Q_1 - E_\gamma}{2048} , \qquad (3.3)$$

where $(E_{pcm} + Q_1 - E_\gamma)$ is the maximum kinetic energy that the first neutron can have.

The energy probability table has a scale of uniform increments of energy associated with a nonuniform scale of probability. The probability "density" is related to the slope of the function at a given point. The problem is then to make random selection of a value of the probability function from that range corresponding to the range of excitation energy available as kinetic energy to an evaporated neutron.

For describing the mechanics of the selection process the following quantities are defined: $E_{ai} = E_{pcm} + Q_1 - E_\gamma$ is the maximum energy available for kinetic energy to the ith neutron to be evaporated; E_{ri} is the energy removed as kinetic energy the the ith neutron; $\Sigma_i E_r$ is the energy removed as kinetic energy by all the neutrons evaporated, previous to the ith one.

The range of excitation energy available as kinetic energy to the ith neutron is defined by

$$J = \frac{E_{ai} - \Sigma_i E_r}{\Delta E} , \qquad (3.4)$$

which is rounded to an integral number. In Fig. 9, the cross-hatched region A corresponds to the range of excitation available for kinetic energy of the ith neutron. The random value of the probability function is obtained by multiplying the quantity $[1.0 - Z(J+1)]$ by a random number between 0 and 1, then adding $Z(J+1)$ again in order to set the absolute value for the random quantity Z(R) correctly. The Z(R) is located in the table of Z between two values Z(N) and Z(N - 1). The randomly chosen kinetic energy for the ith neutron is then

$$E_{ri} = (N-1)\,\Delta E . \qquad (3.5)$$

This procedure continues until there is insufficient excitation energy available for further neutron evaporation. For the cases leading to the particular reaction of interest, the angular distribution is

calculated for the recoiling nuclei; for all other reactions, the total number of cases for each type is recorded.

Within limits of the stated assumptions, the angle Θ which the recoiling nucleus makes with the axis of the projectile particle beam in the laboratory system is

$$\Theta = \tan^{-1} \left\{ \frac{\sqrt{1 - \cos^2 \theta_i}}{\cos \theta_i + \frac{P_a}{P_n}} \right\} , \qquad (3.6)$$

where P_a and P_n are respectively the momentum of the projectile particle and the resultant momentum for i neutrons, and θ is the angle between P_n and the beam axis in the system of the recoiling nucleus. The P_n is computed by adding the momenta of the individual neutrons, using the cosine rule. The isotropic neutron distribution is produced in these calculations by selecting the cosines of the included angles as randum numbers in the range 1 to -1.

The above calculations were performed on an IBM 704 digital computer. The recoil angular distributions were calculated with the energies and other parameters corresponding to conditions of experiment. A program listing in FORTRAN[61, 62] language is given in Appendix A. The table-searching subroutine listing is given in Appendix C. Usually the calculations were made for 5000 cases of the reaction of interest.

The computations produced the following items of information:

(a) The number of recoil events for the reaction of interest, corrected for solid angle, in angular increments corresponding to a given combination of target-to-catcher distance and ring radii.

(b) The total number of each type of neutron evaporation reaction that occurred.

Figure 10 shows the general features of the calculated recoil angular distributions. The shapes of the angular distributions are conveniently discussed in terms of W(1/2), the angle at which the relative differential cross section is reduced to one-half its value at zero degrees. The angle labeled θ-max is the maximum angle to which the recoils can possibly be deflected when the momenta of the evaporated neutrons are all aligned in the same direction and have the maximum possible total kinetic energy.

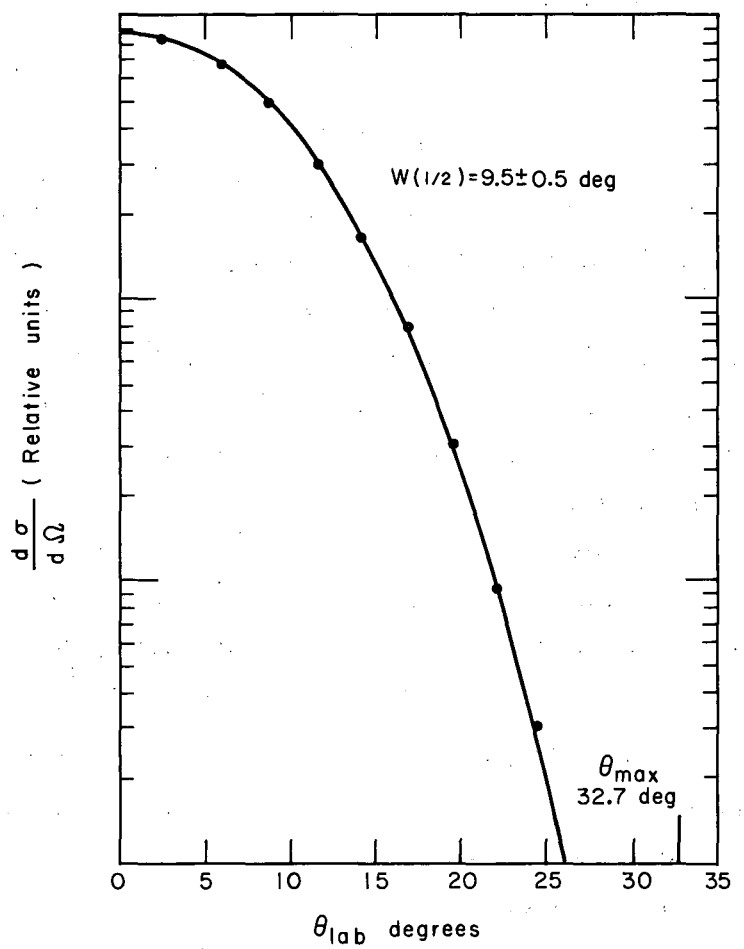

Fig. 10. A typical calculated recoil angular distribution: W(1/2) and θ-max are indicated. For the reaction $Ra^{226}(\alpha, 4n)Th^{226}$, E_α = 42.2 Mev and T = 1.0 Mev.

B. The Nonisotropic Case

The general assumptions and method of neutron-energy selection for the isotropic Monte Carlo calculation apply to this case also, except that in the nonisotropic case it is assumed that the neutrons are evaporated from the recoiling nucleus in a distribution of the form

$$W(\theta)\, d\Omega = (A + B \cos^2\theta)\ d\Omega, \tag{3.7}$$

where $W(\theta)$ is the probability of having a polar angle between θ and $\theta + d\theta$, and A and B are parameters. $W(1/2)$ is insensitive to reasonably gross changes in the ratio B/A; Figure 11 shows that sensitivity is somewhat dependent upon the number of particles evaporated and the momentum of the projectile particle.

The scheme for obtaining random values of θ, weighted by the distribution of Eq. (3.7), is similar to that for selecting the neutron energies except that the range of probabilities is the same for successive neutrons. An integral probability function is obtained by integrating (3.7) to give (see Appendix D-2)

$$R = (A \cos\theta + B/3 \cos^3\theta) + A + B/3\ , \tag{3.8}$$

where R is an integral probability function, illustrated graphically in Figure 12.

This expression is difficult to solve explicitly for a unique θ from a random-chosen value for R, so a 2049-space table was set up for $R[(N - 1)\,\Delta\theta]$, where $\Delta\theta$ is $\pi/2048$. We can then associate a randomly selected value for R with a value for θ. The random value for R is gotten by multiplying the maximum valuefor R, $2(A + B/3)$, by a random number between 0 and 1. The random value is then located in the R table between R(N) and R(N - 1). The corresponding chosen value for θ for the ith neutron is

$$\theta_i = (N - 1)\,\Delta\theta\ . \tag{3.9}$$

The azimuthal angles ϕ_i are obtained by multiplying 2π by a random number between 0 and 1. Random values for θ and ϕ are obtained for each neutron for which an energy has been selected.

The neutron momenta are summed by taking successive projections on the Cartesian coordinates using the relations

$$P_{x,i} = P_{x,i-1} + P_i \sin\theta_i \cos\phi_i\ , \tag{3.10}$$

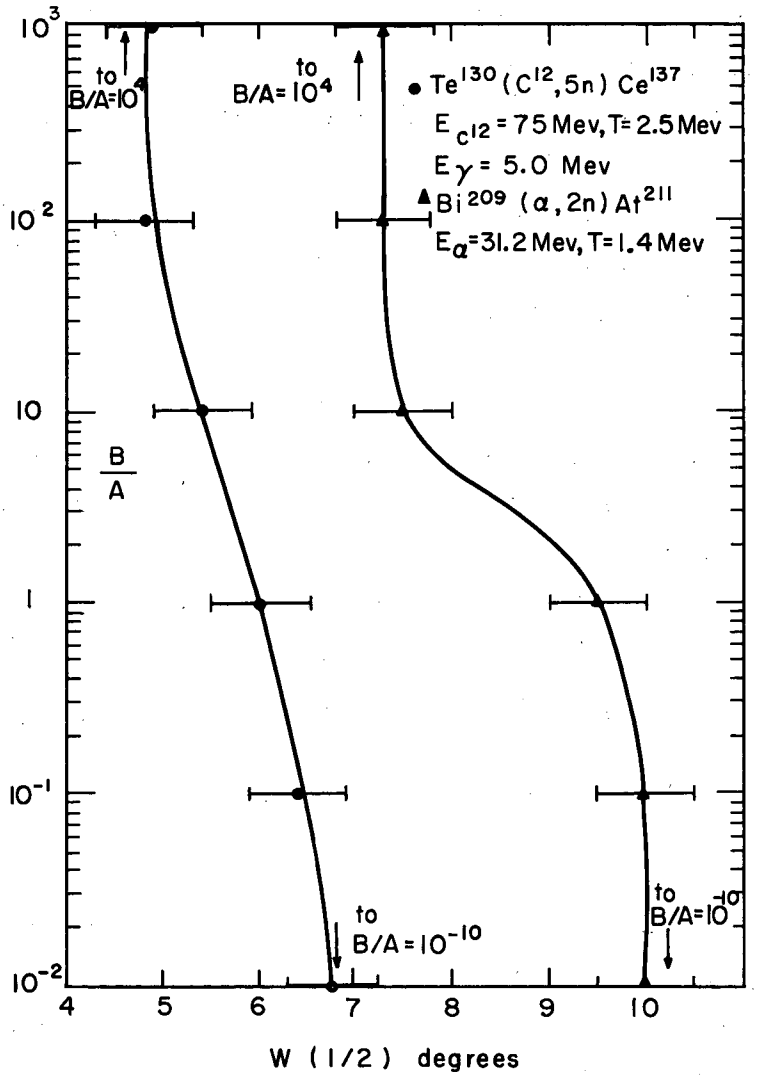

Fig. 11. The variation of W(1/2) as a function of the ratio B/A.

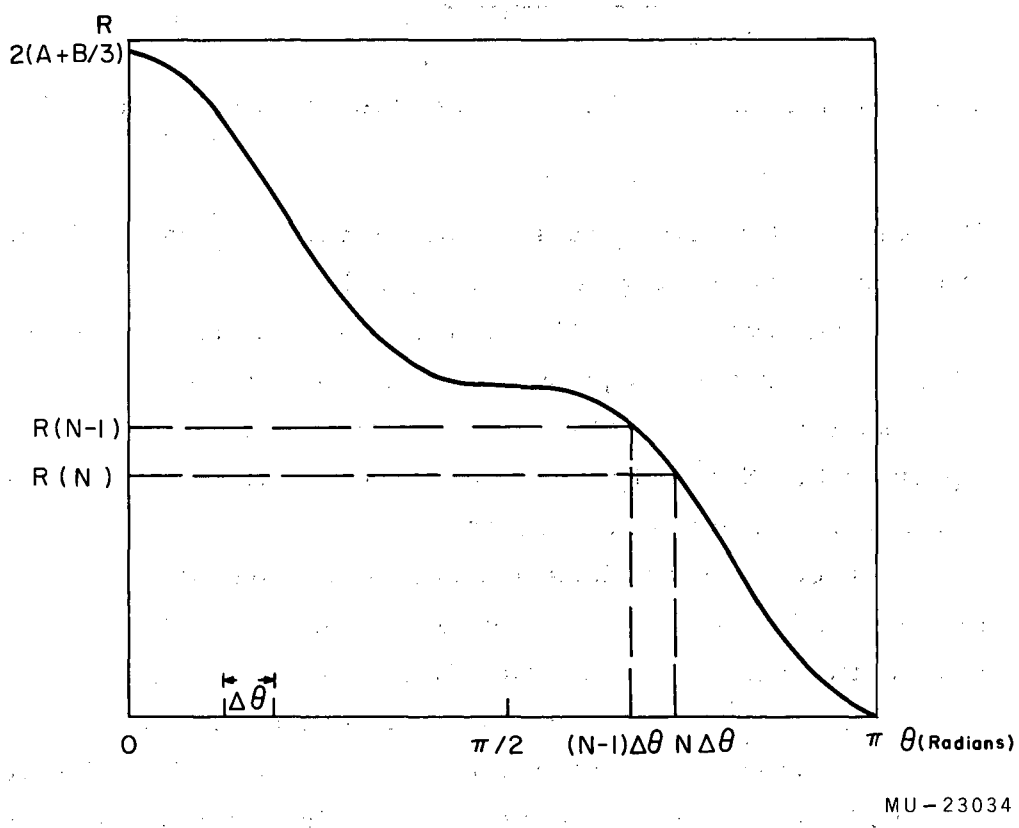

Fig. 12. The integral probability function for selection of the polar angle θ. The scales are greatly expanded.

$$P_{y,i} = P_{y,i-1} + P_i \sin\theta_i \sin\phi_i \,, \tag{3.11}$$

and $$P_{z,i} = P_{z,i-1} + P_i \cos\theta_i \,. \tag{3.12}$$

The final resultant momentum is

$$P_r = \sqrt{P_x^{\,2} + P_y^{\,2} + P_z^{\,2}} \,, \tag{3.13}$$

and its polar angle in the system of the recoiling nucleus is

$$\theta_r = P_z/P_r \,. \tag{3.14}$$

The angle the recoiling nucleus makes with the beam axis in the laboratory system is given by Eq. (3.6).

The nonisotropic Monte Carlo calculation was performed on the IBM 704 computer. A program listing in FORTRAN language is given in Appendix B. The table-searching subroutines are listed in Appendix C. Normally, the calculations were made for 5000 to 10,000 cases of the reaction of interest.

These computations produced the same information listed for the case of isotropic neutron evaporation. In addition, the following information was obtained optionally:

(a) The neutron angular distribution in the system of the recoiling nucleus in angular intervals of $\pi/10$ radian. Figure 13 shows how the large mesh size leads to some distortion of the actual neutron angular distribution — an apparent flattening for the forward and backward angles. Representative neutron angular distributions are shown in Figure 14.

(b) The energy spectra of each of the emitted neutrons for the reaction of interest in energy intervals of 0.2 Mev. Figures 15 and 16 show representative neutron energy distributions.

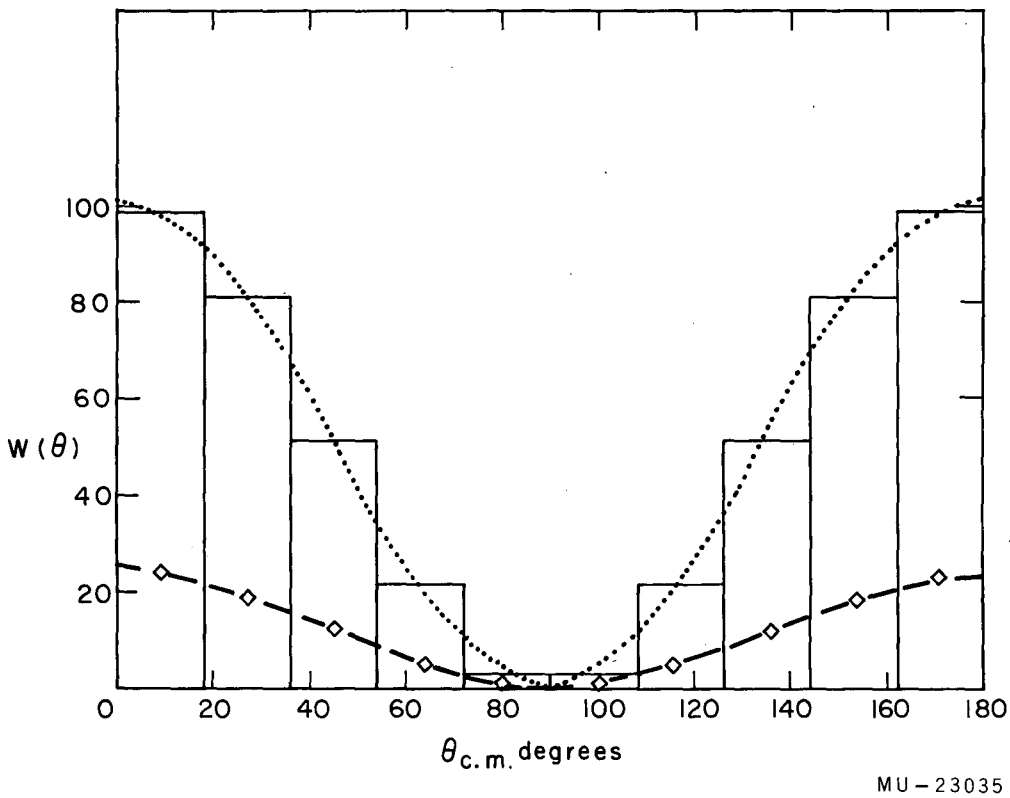

Fig. 13. Plot of the neutron angular distribution $W(\theta) = A + B(\cos^2\theta)$ in the system of the recoiling nucleus for $B/A = 100$. The dotted line is the actual distribution; the solid lines are the histogram from the mesh size; the dashed line is obtained by integrating the histograms; points are from the computations.

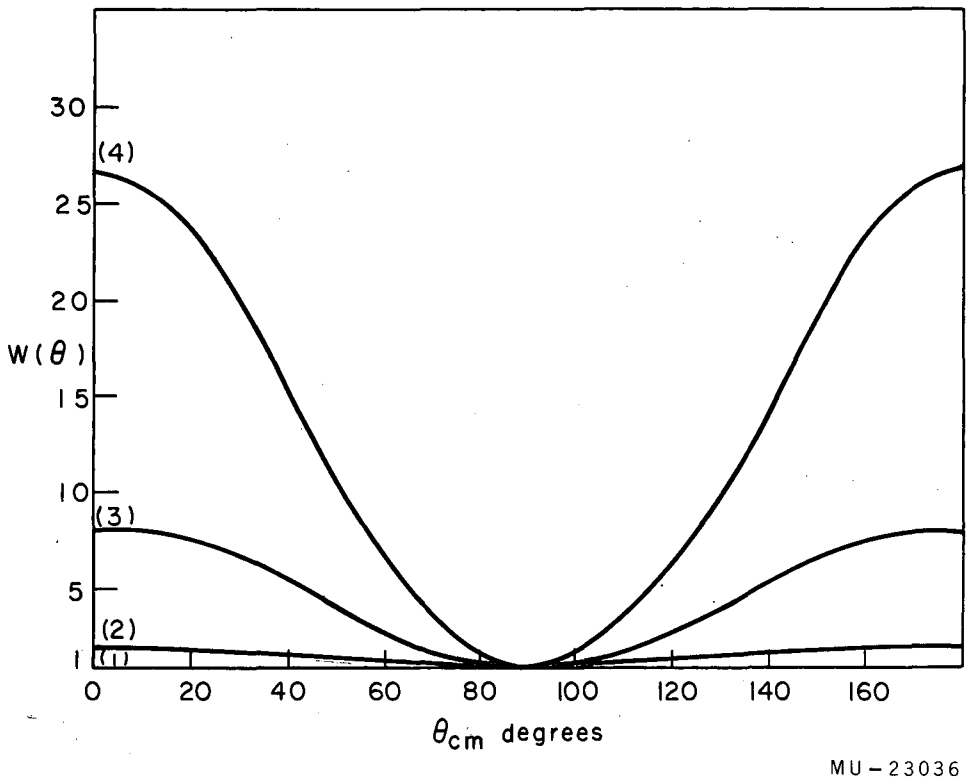

Fig. 14. Plot of the neutron angular distributions for various values of B/A: (1) 10^{-10}, (2) 1, (3) 10, (4) 100.

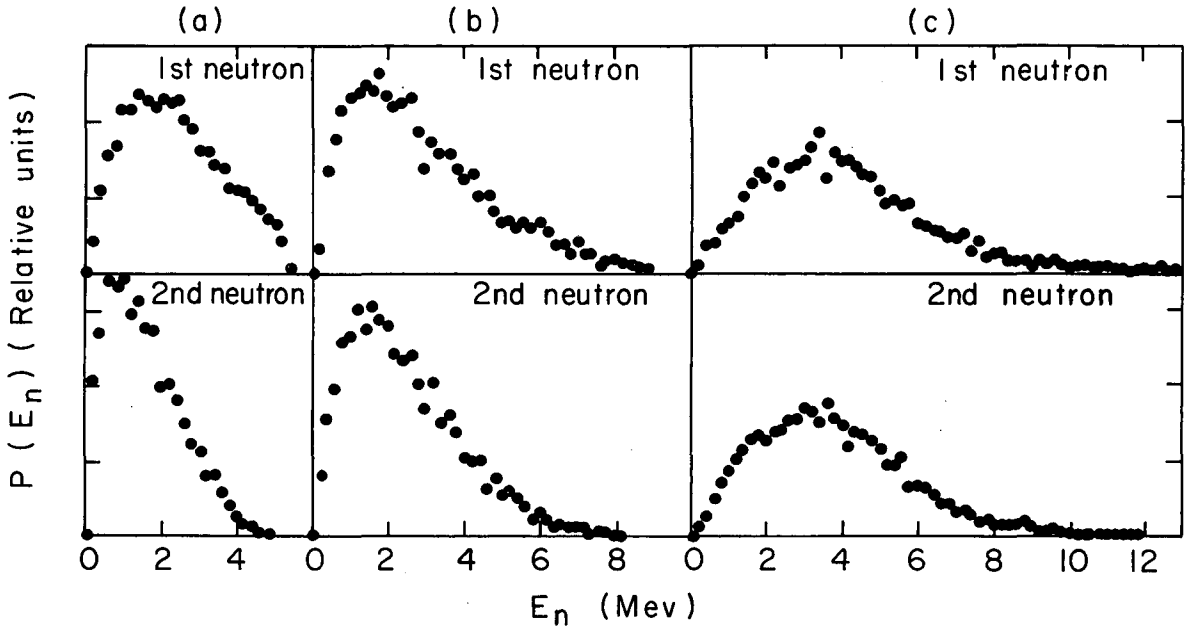

MU-23037

Fig. 15. Calculated neutron energy spectra for the reaction $Pb^{208}(\alpha, 2n)Po^{210}$, T = 1.45 Mev and $E_{\alpha(c.m.)} + Q_2$ = (a) 5.1 Mev, (b) 8.7 Mev, and (c) 12.9 Mev.

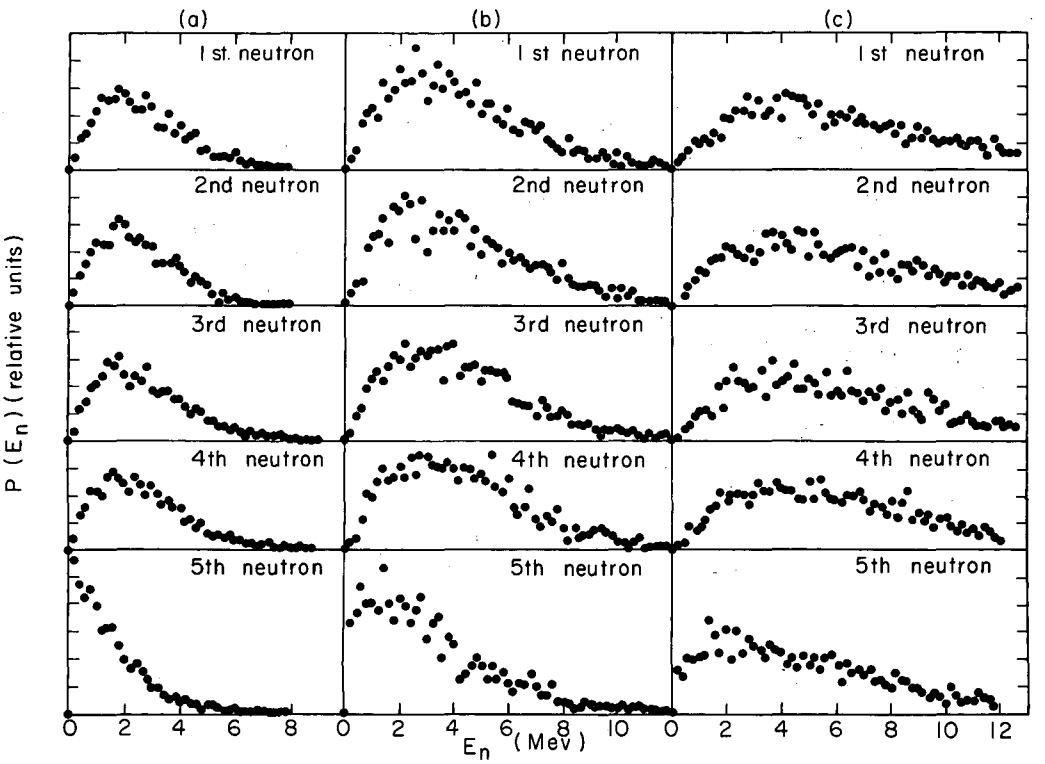

Fig. 16. Calculated neutron energy spectra for the reaction $Te^{130}(C^{12}, 5n)Ce^{137}$, T = 2.5 Mev, E_γ = 5.0 Mev, and $E_{C^{12}} + Q_5$ = (a) 18 Mev, (b) 28 Mev, and (c) 39 Mev.

C. Discussion of Monte Carlo Calculations

The information above suggests several conclusions about the various parameters of the Monte Carlo calculations:

1. Anisotropy

Figure 11 shows that the calculations are fairly insensitive to the value of B/A. Up to $B/A \approx 0.2$ for C^{12} reactions and $B/A \approx 1.0$ for alpha-induced reactions, the W(1/2) values do not depart appreciably from those expected from an isotropic distribution for evaporated neutrons. Hence it is apparent that agreement of experimental distributions with a calculation of this type is not necessarily indicative of neutron emission according to precise values for B/A; moderate ranges of anisotropy could not be distinguished from the isotropic case. Also, isotropy of neutron emission could not be established by this means.

It is recognized, of course, that a distribution of the form $A + B \cos^2\theta$ is incapable of representing strong forward-backward anisotropies. For such cases, the form $(\sin\theta)^{-1}$ is more appropriate;[63, 64] however, the $(\sin\theta)^{-1}$ distribution is not considered to be applicable in this case.[63, 65]

2. Nuclear Temperature

Figure 7 shows that the assumption of constant nuclear temperature is not unreasonable for this purpose, although in general, such an assumption is not believed to be valid.[66-68] Consider as an example the $Te^{130} + C^{12}$ system, forming a compound nucleus with an initial excitation energy of about 70 Mev. For each neutron-evaporation step, one can estimate the temperature of the residual nucleus by

$$T = \sqrt{\frac{10.5\ E}{A}},$$

where E and A are the excitation energy and mass number of the residual nucleus.[68] As five neutrons are successively emitted, these estimated temperatures decrease from about 2.0 to 1.5 Mev, virtually constant in the level of approximation of the Monte Carlo calculations.

A related aspect of this problem is seen in the calculated neutron evaporation spectra of Figs. 15 and 16. Within the limited statistical accuracy some interesting qualitative trends appear:

(a) For a given excitation energy, all the neutrons evaporated in one cascade have approximately the same energy spectra except for the last one, which is usually shifted to lower energy. This is caused by the restrictions on the energy available to the last neutron.

(b) For increased excitation energy in the system there is a general shift in the peaks of all the spectra to somewhat higher energies.

3. Excitation Not Removed by Neutron Emission: E_γ

The sensitivity of the parameter E_γ is shown in Figure 8. It is perhaps physically unreasonable to use a single value rather than some distribution of values for this quantity in a given calculation. This was done arbitrarily to avoid undue complexity. It is believed that this assumption may cause the calculated recoil angular distributions to be unrealistically narrowed near θ-max; however, at angles from 0 deg to the neighborhood of W(1/2), the more probable values from a distribution should dominate.

4. Effect of Angular Resolution

Figure 13 shows the extreme distortion that can be caused by use of a very coarse angular mesh size for the neutron angular distributions. The effect of angular resolution was also considered for the recoil angular distributions; in this case the angular increments were much smaller.[69, 70] Calculations were performed for target-to-catcher spacings of 4.0 and 10.0 cm with other conditions unchanged; this corresponds to a reduction in the angular mesh by a factor of 2.5. This change produced improvement in angular resolution at small angles, but the recoil angular distributions defined by each set of points were essentially identical. This means that moderate variations in the mesh size are not particularly important. In practically every case, calculations were compared with experiments having the same angular resolution.

IV. RESULTS

The recoil angular distributions calculated by the Monte Carlo method form a basis for comparison with experiment. Agreement between calculations and experiment lends support to the compound-nucleus-statistical-model description of these reactions. The recoil-range measurements provide more direct information about the extent of momentum transfer. Normally, formation of a compound nucleus is expected to lead to recoiling products with the maximum attainable kinetic energy although a few exceptions have been reported.[71] The range of the recoils is known to be an increasing function of their energy.[3]

Comparisons of calculated and the experimental recoil angular distributions are summarized below in plots of W(1/2) vs $E_{pcm} + Q$, the energy available to evaporated neutrons. It should be emphasized that agreement between the distributions is not judged solely by agreement between the magnitudes of the W(1/2) values, but by a detailed comparison of the two distributions from 0 deg to angles in the neighborhood of W(1/2). Such a favorable comparison is illustrated in Figure 17. The departure of the experimental points from the smooth curve at wider angles is attributed to scattering from the surface of the target or from gas molecules in the evacuated chamber.

The experimental recoil ranges are examined in terms of the theoretical treatment, which considers the mean recoil range to be proportional to its energy, E_r, for $A_r \gg A_s$:[72]

$$R_0\ (\mu g/cm^2) = 602\ E_r\ \frac{A_s\ (A_s + A_r)}{A_r}\ \frac{\sqrt{Z_s^{2/3} + Z_r^{2/3}}}{Z_s\ Z_r}\ . \qquad (4.1)$$

Here A and Z are the charge and mass numbers, the subscripts s and r refer respectively to the stopping and recoil atoms, and E_r in the case of compound-nucleus formation is defined by[73]

$$E_r = \frac{E_p\ A_p\ A_r}{(A_p + A_t)^2}\ , \qquad (4.2)$$

where the subscripts p, r, and t refer to the projectile, recoil, and target. Theoretically, the distribution about the mean range R_0

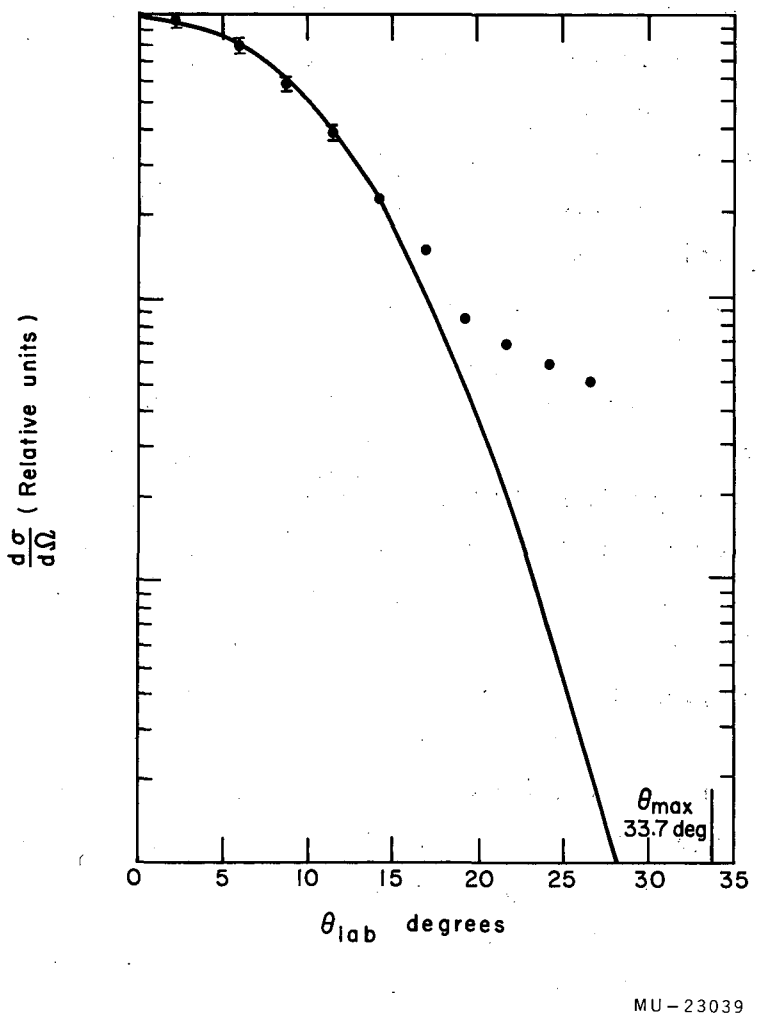

Fig. 17. Comparison of experimental and Monte Carlo recoil angular distributions for $Ra^{226}(\alpha, 4n)Th^{226}$. The curve is drawn to fit the Monte Carlo calculation for E_α = 43.2 Mev, T = 1.0 Mev, E_γ = 0. Experimental points are shown for the same bombarding energy.

is expected to be of Gaussian form with the standard deviation parameter, σ, expressed by ρR_0.[74] The "straggling parameter" ρ is expected to have a value given by[75]

$$\rho = \left(\frac{2 A_s A_r}{3(A_s + A_r)^2} \right)^{1/2} . \tag{4.3}$$

This theoretical framework is well supported by experiment.[3]

A comprehensive discussion of recoil ranges is presented in Ref. 73.

The recoil angular distribution and range results follow, grouped together for each particular set of reactions. The results of Monte Carlo calculations for the recoil angular distributions are tabulated in Appendix E.

A. $Ra^{226}(\alpha, 4n)Th^{226}$

The experimental and calculated recoil angular distributions are compared in Figure 18. The general features of this curve have been interpreted[1] to mean that, as the excitation energy increases above the reaction threshold, there is an increase in the momentum given to the residual nucleus by the emitted neutrons; at energies near the peak of the excitation function the emitted neutrons have approximately the same energy; and at energies beyond the peak of the excitation function the reaction occurs only when the emitted neutrons have relatively higher energies, owing to competition from the reaction which causes an additional neutron to be evaporated. The experimental recoil angular distributions are summarized in Table III.

A typical differential recoil range curve is shown in Figure 19. These range curves were fitted to Gaussian distributions by use of probability plots from which the mean range R_0 and the standard deviation σ could be determined.[76] Such a plot is shown in Figure 20. The measurements of the Th^{226} recoil ranges in hydrogen are summarized in Figure 21 and Table IV. The E_r values are based on the assumption that a compound nucleus is formed.

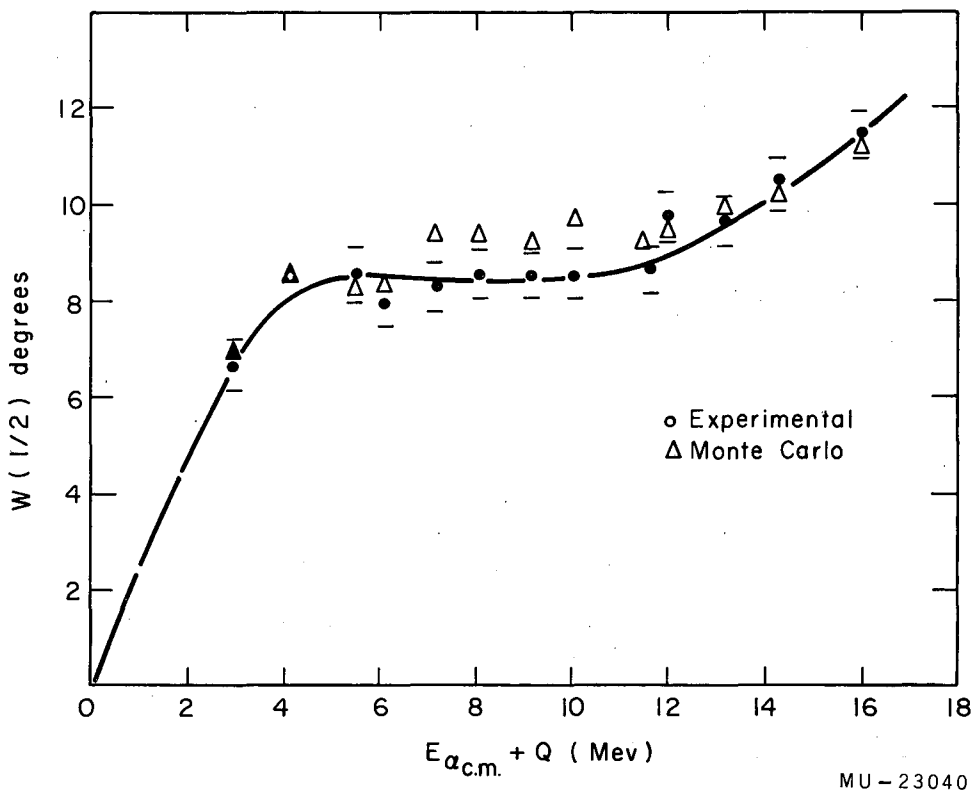

Fig. 18. Plot of W(1/2) as a function of $E_{\alpha(c.m.)} + Q$, the energy available as kinetic energy of the emitted neutrons, for $Ra^{226}(\alpha, 4n)Th^{226}$.

TABLE III. Summary of experimental recoil angular distribution data[a] — $Ra^{226}(\alpha, 4n)Th^{226}$

E_α Mev	W(1/2)[b] Degrees	Relative $d\sigma/d\Omega$, for angles in degrees[69]									
		2.31	5.97	8.71	11.47	14.24	16.88	19.38	21.85	24.23	26.57
32.9	6.7	89	54	27	4.0						
35.5	8.6	35	29	19	12	7.5	4.0	2.7			
36.1	8.0	88	68	42	29	16	10	5.6	1.3		
37.2	8.3	62	46	32	20	9.0	7.0	3.7	2.8		
38.2	8.6	58	44	31	20	11	8.0	5.1	4.8		
39.3	8.6	90	68	47	31	16.5	10	5.3	3.3		
40.2	8.6	45	34	24	15	8.5	6.0	3.9	3.3		
41.9	8.7	98	74	51	34	19	11.5	6.6	5.5		
42.2	9.8	64	52	39	28	17.5	10.5	5.8	3.4	2.2	
43.2	9.7	44	36	26	18	10	6.8	3.8	3.2	2.7	
44.5	10.5	66	59	44	31	17	13	7.6	5.1	4.1	3.5
46.2	11.5	39	32	27	20	14	9,5	6,0	4.0	3.1	2.2

[a] Errors due to counting statistics are $\lesssim \pm 2\%$.

[b] The overall error in W(1/2) is estimated to be $\lesssim \pm 0.5$ deg.

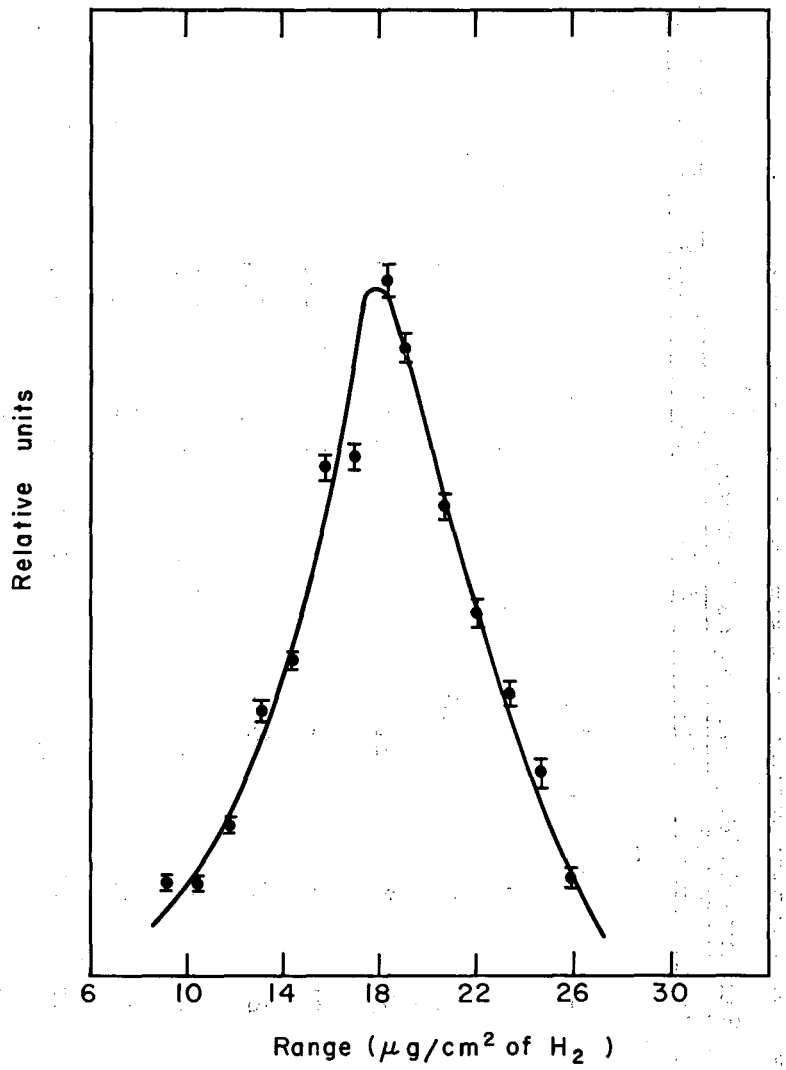

Fig. 19. Differential range curve for Th^{226} recoils in hydrogen; E_α = 41.6 Mev.

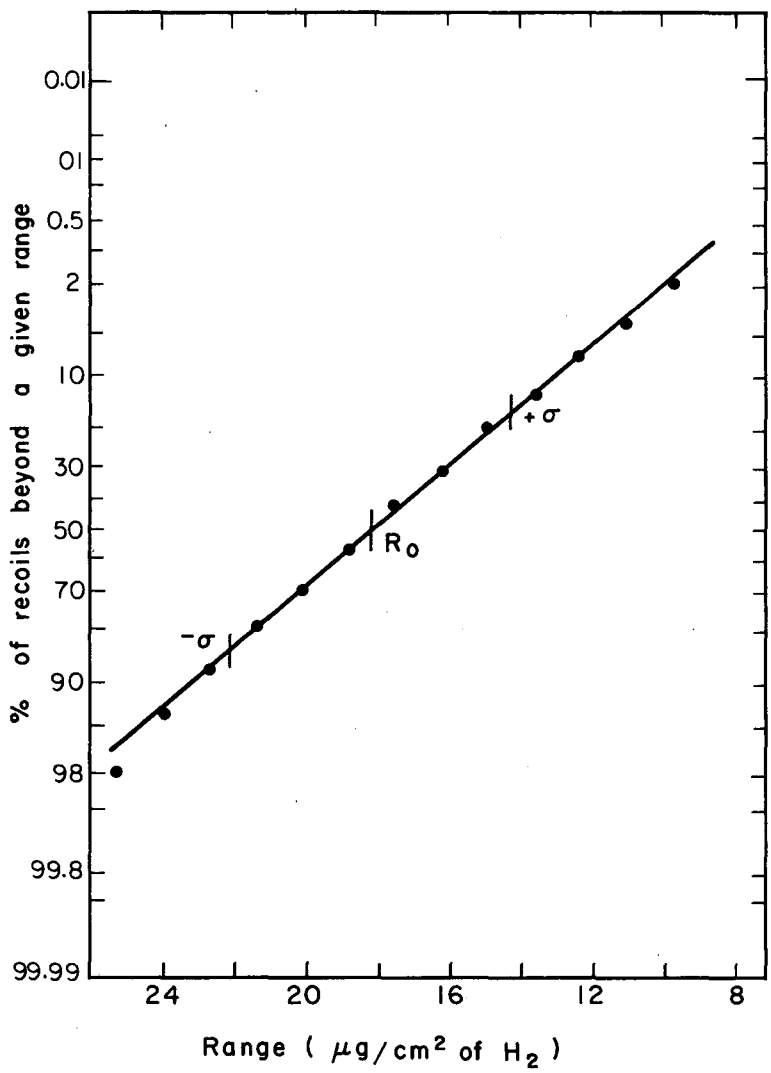

MU-23042

Fig. 20. Probability plot of Th^{226} recoil ranges in hydrogen for E_α = 41.6 Mev. The points $-\sigma$, $+\sigma$, and R_0 are indicated on the plot. In this case, R_0 = 18.2 $\mu g/cm^2$ and σ = 3.92 $\mu g/cm^2$.

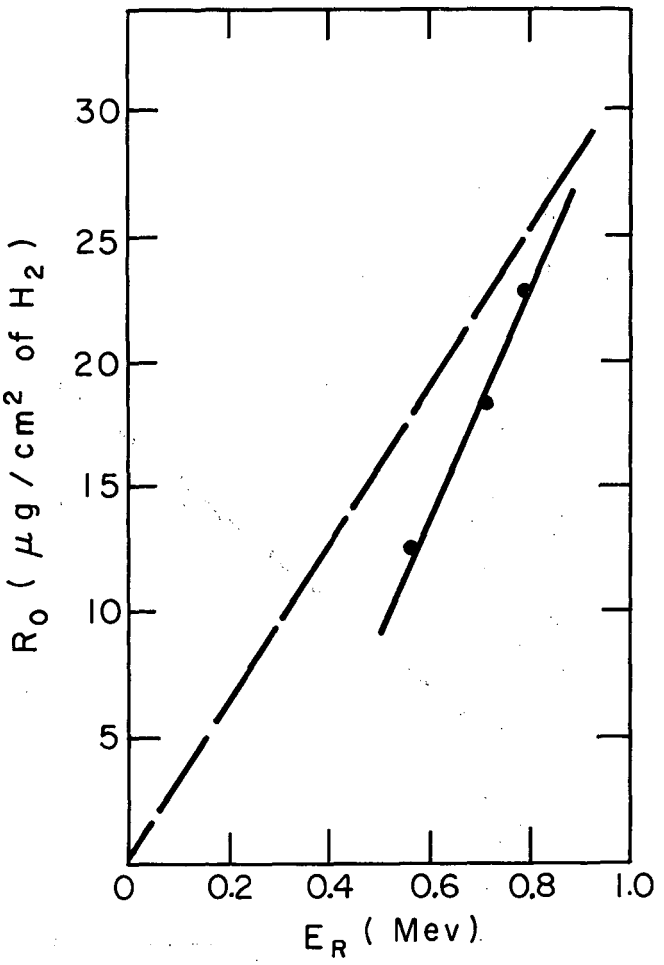

MU-23043

Fig. 21. Range of Th^{226} recoils in hydrogen as a function of the energy of the recoil (solid line). The broken line is the theoretical range-energy curve.

TABLE IV. Summary of $Ra^{226}(\alpha, 4n)Th^{226}$ recoil range data

E_α Mev	E_r Mev	R_0, Exptl. $\mu g/cm^2$ H_2	R_0, Theoretical $\mu g/cm^2$ H_2	ρ Exptl.	ρ Theor.	σ exptl. $\mu g/cm^2$
34.1	0.584	13.5	18.4	0.266	0.0542	3.35
41.6	0.710	18.2	22.4	0.215	0.0542	3.92
46.2	0.790	23.2	24.9	0.195	0.0542	4.45

B. $Pb^{208}(\alpha, 2n)Po^{210}$

Comparison between the experimental and Monte Carlo recoil angular distributions is shown in Figure 22. The experimental recoil distributions are summarized in Table V.

The experimental data from the thick-target recoil range studies with natural Pb + He^4 are presented in Figure 23 and Table VI.

C. $Pb^{207}(\alpha, n)Po^{210}$

The recoil angular distribution data for this system cannot be compared conveniently in terms of W(1/2) because of the structure in the curves. Representative experimental and calculated curves are compared in Figure 24. The experimental distributions are summarized in Table VII. Monte Carlo distributions for several values for T are given in Appendix E.

D. $Te^{130}(C^{12}, 5n)Ce^{137m}$

In Figure 25 the W(1/2) values for experiment are compared with calculated ones for the isotropic case, and for the nonisotropic case where best fits are obtained by using B/A = 1.2 and various combinations of T and E_γ, listed in Table VIII. Selection of the value for B/A is discussed later. The experimental angular-distribution data are listed in Table IX. Monte Carlo data are given in Appendix E.

A typical histogram for the recoil range data from natural Te + C^{12} is illustrated in Figure 26. The Gaussian fit by the probability plot is given in Figure 27 for same set of data. The recoil range data are compared in Figure 28 to a range-energy curve calculated for Ce recoils by adjusting the published values for Tb^{149} for differences in Z and A.[73] The E_r values are calculated by assuming formation of a compound nucleus. The experimental recoil range data are summarized in Table X.

E. $Pr^{141}(C^{12}, 4n)Tb^{149}$

The experimental and Monte Carlo recoil angular distributions are compared in Figure 29. The experimental data are summarized in Table XI.

Excellent recoil range data for this reaction have been published by Winsberg and Alexander.[73]

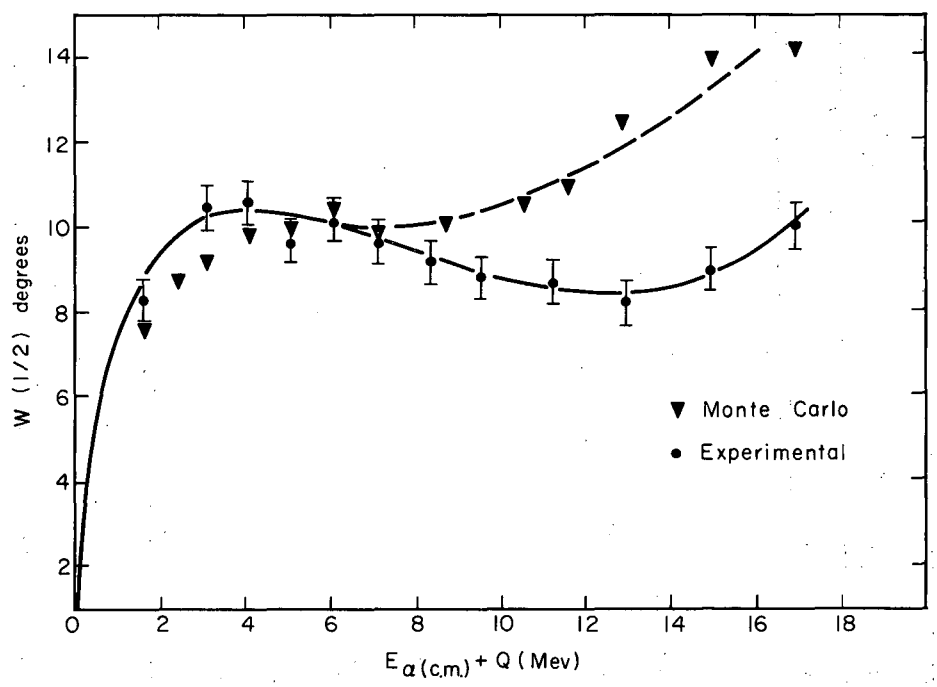

MU-23044

Fig. 22. Plot of W(1/2) as a function of $E_{\alpha(c.m.)} + Q$ for $Pb^{208}(\alpha, 2n)Po^{210}$. The solid line is drawn through the experimental points; the dashed line is drawn through the calculated points.

TABLE V. Summary of experimental recoil angular distribution data[a] - $Pb^{208}(\alpha, 2n)Po^{210}$

E_α Mev	W(1/2)[b] Degrees	Relative $d\sigma/d\Omega$, for angles in degrees[69]								
		2.31	5.97	8.71	11.47	14.24	16.88	19.38	21.85	24.23
21.7	8.3	89	72	42	13					
23.1	10.5	91	80	62	36	12	1.2			
24.0	10.7	90	82	66	41	7				
25.1	9.7	96	83	59	27					
26.2	10.2	96	86	63	34					
27.2	9.6	98	85	60	30	2.5				
28.4	9.2	96	82	55	11					
29.7	8.8	97	80	50	16					
31.7	8.7	94	75	48	18					
33.0	8.2	92	68	46	21	8.4	2.8	0.7		
35.2	9.0	86	68	48	30	12.5	5.0	1.5		
37.2	10.0	85	67	54	40	24	16	8.0	4.0	1.9

[a] Errors due to counting statistics are $\lesssim \pm 2\%$.

[b] The overall error in W(1/2) is believed to be $\leqslant \pm 0.5$ deg.

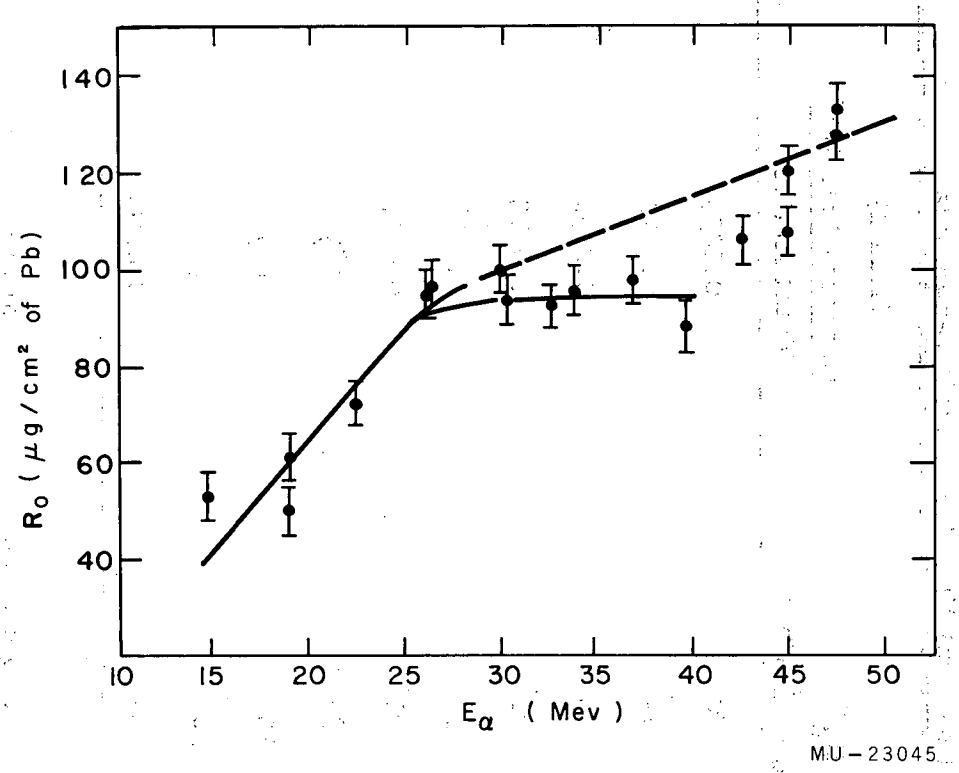

Fig. 23. Plot of mean recoil range as a function of bombarding energy for natural Pb+He^4. The solid line is drawn through the points representing probable products from the (α, 2n) reaction. The broken line crudely represents the range curve that might be expected for a compound-nucleus mechanism.

TABLE VI. Summary of natural Pb + He^4 recoil range data

E_α Mev	(Run 1) Catcher-Activity[a] / Total Activity	R_0[b] $\mu g/cm^2$ Pb	(Run 2) Catcher-Activity[a] / Total Activity	R_0[b] $\mu g/cm^2$ Pb
19.0	0.0089	50	0.0095	53.2
22.3	0.0128	72	0.0110	61.5
26.3	0.0169	95	0.0130	73
30.1	0.0176	99	0.0173	97
33.6	0.0165	92	0.0168	94
36.8	0.0176	99	0.0172	96
39.7	0.0158	88.5	([c])	-
42.3	0.0191	107	([c])	-
44.9	0.0192	108	([c])	-
47.4	0.0239	134	0.0220	128

[a] Counting errors were $\leqslant$ 4%.

[b] The uncertainty due to variations in target thickness is estimated to < 5%.

[c] These foils were damaged by overheating.

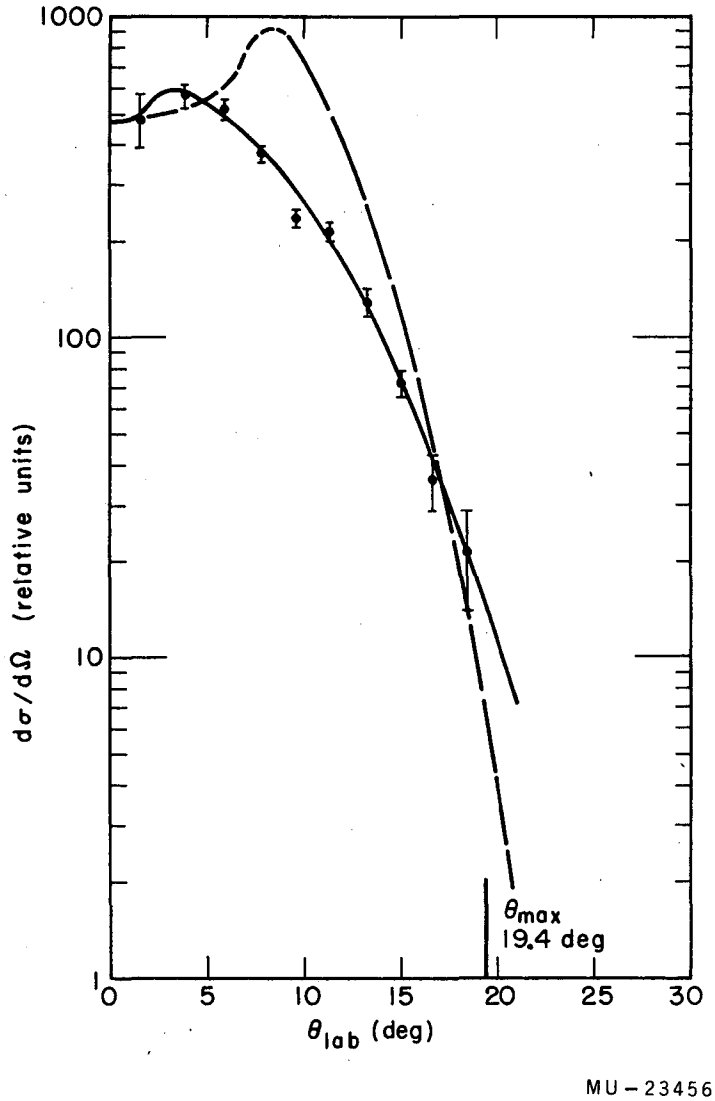

Fig. 24. Comparison between experimental (solid curve) and Monte Carlo (dashed curve) recoil angular distributions for $Pb^{207}(\alpha, n)Po^{210}$ at E_α = 22.3 Mev. Calculation uses T = 1.4 Mev.

TABLE VII. Summary of experimental recoil angular distribution data — $Pb^{207}(\alpha, n)Po^{210}$

E_α Mev	Relative $d\sigma/d\Omega$, for angles in degrees									
	2.32[69]	5.97	8.71	11.47	14.24	16.88	19.38	21.85	24.23	26.57
19.7	.17[a]	0.22	0.13	0.09	0.05	0.03	0.05	0.02	0.0	0.02
21.7	1.71[b]	1.50	1.08	0.60	0.28	0.13	0.03			
	1.54[70]	3.99	5.84	7.70	9.61	11.44	13.20	14.97	16.71	18.44
22.3	0.66[c]	0.80	0.73	0.52	0.33	0.30	0.18	0.10	0.05	0.03
24.0	0.59[d]	0.64	0.51	0.39	0.13	0.15	0.03			

[a] Total error estimated $\leqslant$ 15% to 14.24 deg.

[b] Total error estimated $\leqslant$ 8% to 11.47 deg.

[c] Total error estimated to be 21% for first point, $\leqslant$ 8% for other points to 9.61 deg.

[d] Total error estimated to be $\leqslant$ 19% to 7.70 deg.

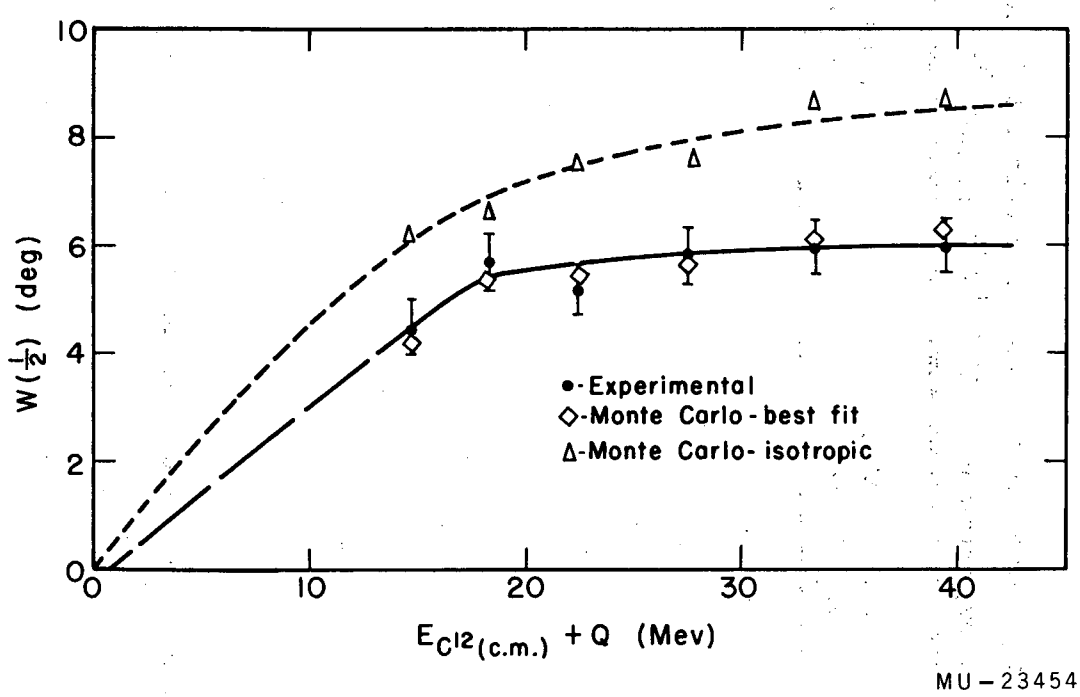

Fig. 25. Plot of W(1/2) vs $E_{C^{12}(c.m.)}$ + Q for $Te^{130}(C^{12}, 5n)Ce^{137m}$. Solid line is fitted to experimental points. Dotted line fits the case for $B/A \rightarrow 0$, $E_\gamma = 0$ (isotropic case).

TABLE VIII. Summary of parameters for best fit of calculated recoil angular distributions to experiment — $Te^{130}(C^{12}, 5n)Ce^{137m}$

$E_{C^{12}}$ Mev	T = 2.5 Mev E_γ (Mev)	T = 1.5 Mev E_γ (Mev)
59.0	5	5
64.5	6	6
69.0	7	8
75.0	8	8
81.0	11	8
87.5	15	11

TABLE IX. Summary of experimental recoil angular distribution data – $Te^{130}(C^{12}, 5n)Ce^{137m}$

$E_{C^{12}}$ Mev	W(1/2)[a] Degrees	Relative $d\sigma/d\Omega$, for angles in degrees									
		1.54[70]	3.99	5.84	7.70	9.61	11.44	13.20	14.97	16.71	18.44
59.0	4.5	59[b]	23	14.5	9.5	4.1	2.6	1.4	1.0	0.78	0.52
64.5	5.6	67[c]	49	36	14	6.8	4.0	1.7	0.78	0.38	
69.0	5.2	17[d]	12.5	7.2	4.5	2.4	1.5	1.1	0.65	0.40	0.39
81.0	6.0	64[d]	48	36	24	12.5	8.5	5.0	4.2	4.8	
87.5	6.2	52[d]	37	29	21	11	11	8.5	4.5	6.7	5.2
		2.31[69]	5.97	8.71	11.47	14.24	16.88	19.38	21.85	24.23	
74.5	5.8	51[e]	27	14	9.5	3.5	2.5	2.0	1.3		

[a] The overall error in W(1/2) is estimated to be $\leqslant \pm 0.5\%$.

[b] Overall errors are estimated to be $\leqslant 5\%$ to 9.61 deg.

[c] Overall errors are estimated to be $\leqslant 3\%$ to 9.61 deg.

[d] Overall errors are estimated to be $\leqslant 6\%$ to 7.70 deg.

[e] Overall errors are estimated to be $\leqslant 4\%$.

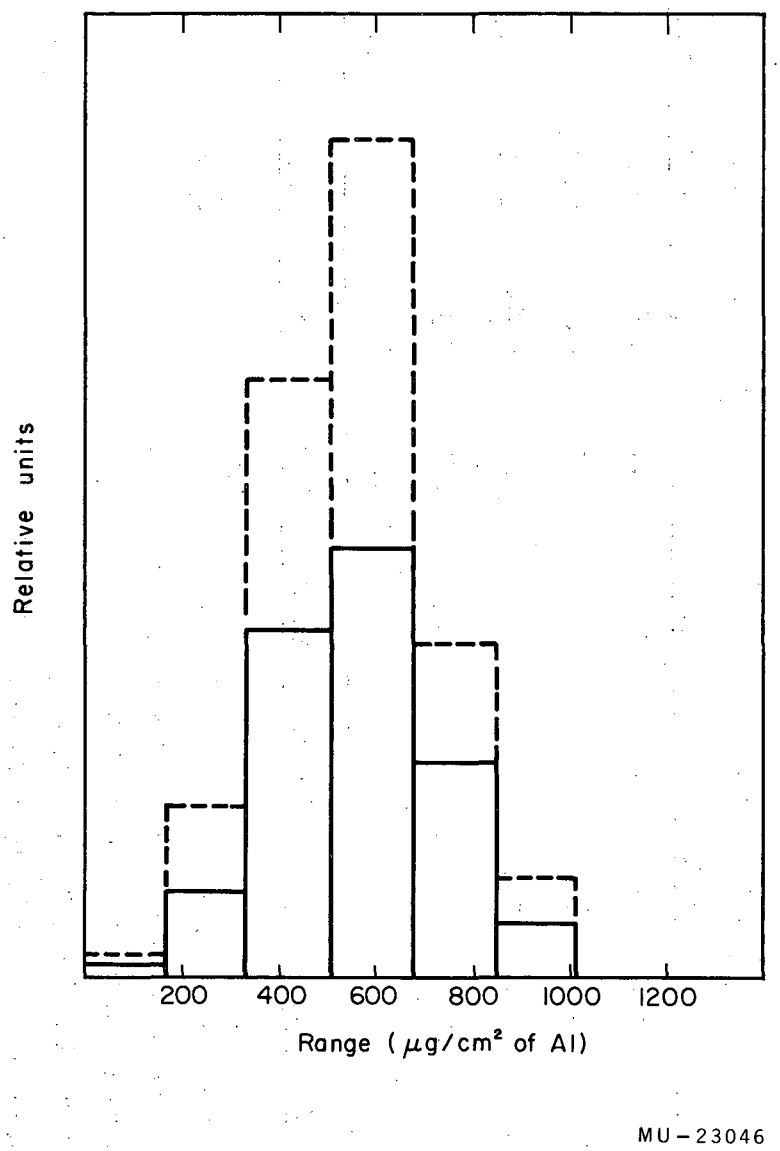

Fig. 26. Histogram for the ranges of the recoiling Ce and La products of natural $Te+C^{12}$ at $E_{C^{12}} = 90$ Mev. The solid lines indicate the long-lived group; the dashed lines indicate the short-lived group.

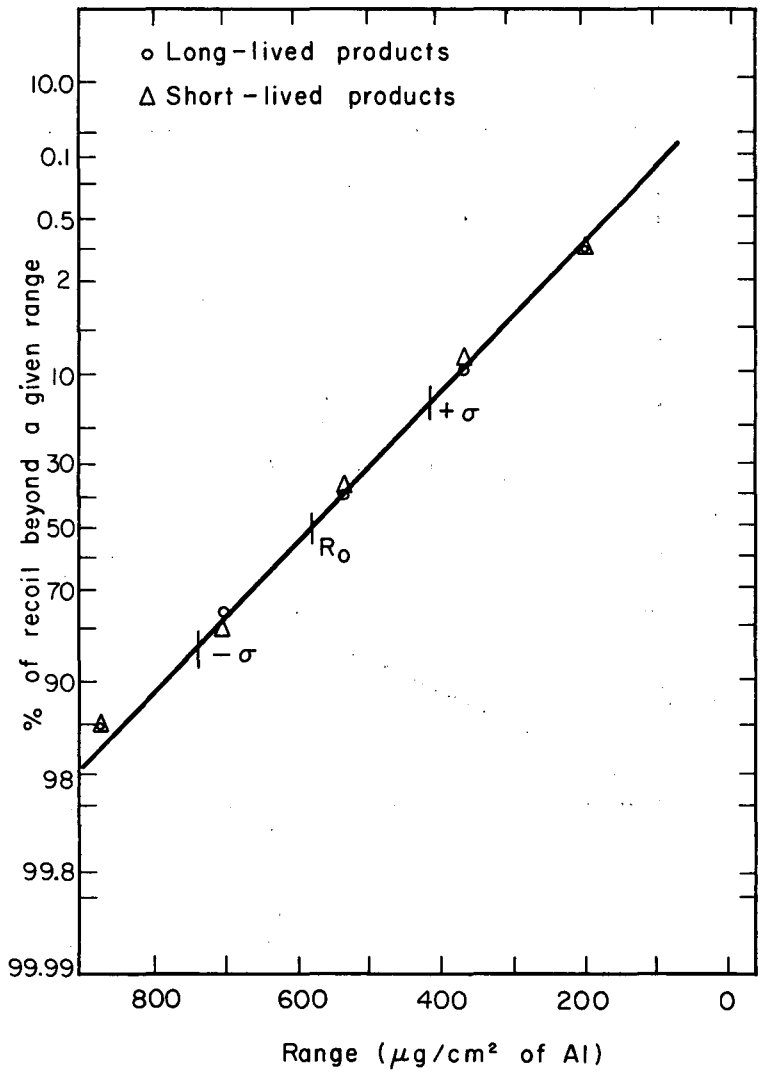

MU-23047

Fig. 27. Probability plot of Ce and La recoil ranges in aluminum for $E_{C^{12}} = 90$ Mev. The points $-\sigma$, $+\sigma$, and R_0 are indicated. In this case $R_0 = 580\ \mu g/cm^2$ and $\sigma = 162\ \mu g/cm^2$.

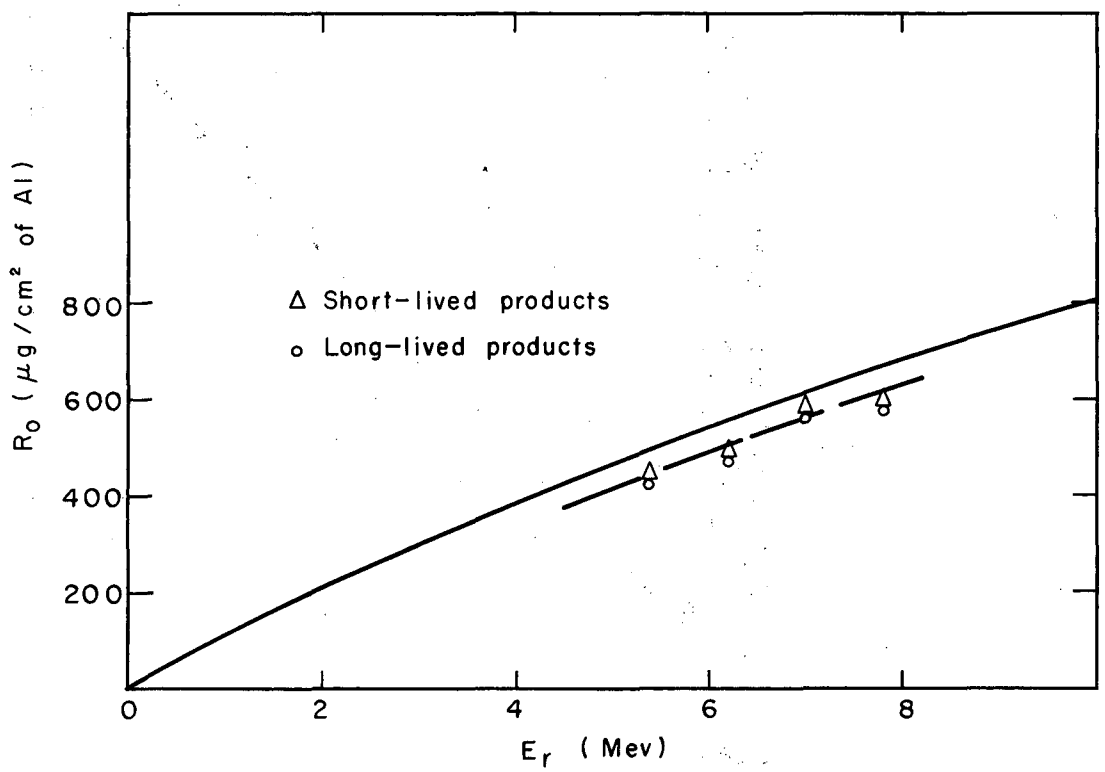

MU-23048

Fig. 28. Range-energy curve for the recoiling Ce and La products from the reactions of natural Te + C^{12}. The experimental points are compared with a solid curve calculated from the Tb^{149} range of Reference 73.

TABLE X. Summary of natural Te $+C^{12}$ recoil range data

$E_{C^{12}}$ Mev	E_r Mev	Group	Expt. R_0 $\mu g/cm^2$ Al	R_0 from Tb^{149} Data ($\mu g/cm^2$ Al)	ρ Exptl.	ρ Theor.	Exptl. σ $\mu g/cm^2$
70	5.40	Long-lived	428	493	0.339	0.304	145
		Short-lived	435	493	0.333	0.304	145
80.3	6.20	Long-lived	475	554	0.280	0.304	133
		Short-lived	482	554	0.276	0.304	133
90	6.95	Long-lived	580	610	0.279	0.304	162
		Short-lived	580	610	0.279	0.304	162
99.5	7.70	Long-lived	580	660	0.283	0.304	164
		Short-lived	590	660	0.276	0.304	163

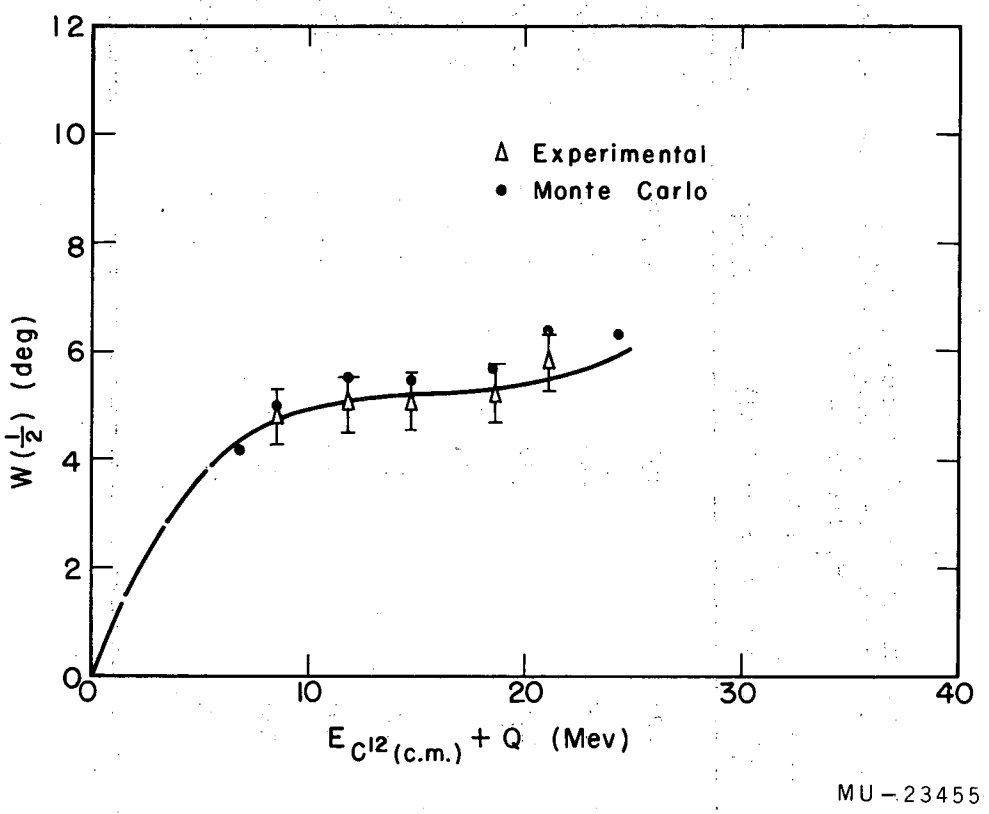

Fig. 29. Plot of W(1/2) versus $E_{C^{12}(c.m.)} + Q$ for $Pr^{141}(C^{12}, 4n)Tb^{149}$.

TABLE XI. Summary of experimental recoil angular distribution data – $Pr^{141}(C^{12}, 4n)Tb^{149}$

$E_{C^{12}}$ Mev	W(1/2)[a] Degrees	Relative $d\sigma/d\Omega$, for angles in degrees[70]								
		1.54	3.99	5.84	7.70	9.61	11.44	13.20	14.97	16.71
58.0	4.8	92[b]	61	36	16	5.4	1.9	0.8	0.27	
61.5	5.0	95[c]	66	39	19	6.2	2.3	0.9	0.43	
64.5	5.1	94[b]	70	38	20	6.4	2.8	0.7	0.3	
69.5	5.2	95[c]	68	42	22	6.2	2.7	0.9	0.4	
71.5	5.8	94[b]	70	49	29	10	5.7	1.8	1.1	0.5

[a] The overall error in W(1/2) is estimated to be $\leqslant \pm 0.5\%$.

[b] Errors due to counting statistics are $\leqslant$ 6% to 7.70 deg.

[c] Errors due to counting statictics are $\leqslant$ 3% to 7.70 deg.

V. DISCUSSION

The recoil angular distribution and range data listed in the preceding section, together with the experimental excitation functions, furnish fairly direct information about many features of the nuclear reaction mechanisms.

In the following discussion the reactions studied are classified into two general groups: those which can be fitted by the simple isotropic Monte Carlo calculation and those which either require special treatment or cannot be fitted at all.

A. Reactions That Can Be Fitted By the Calculations

1. $Pr^{141}(C^{12}, 4n)Tb^{149}$

Figure 29 shows that the experimental recoil angular distributions agree quite closely with the simple isotropic Monte Carlo calculation using $E_\gamma = 0$ and $T = 1.5$ Mev. This value for T was obtained by Jackson fit to Alexander's experimental excitation function.[77] It was shown in Figure 7 that the precise choice for T should not be critical for the result of the Monte Carlo calculation.

The maximum measured cross section for this reaction is about 35 mb.[77]

Recoil range data for Tb^{149} from this and a number of other reactions have recently been published by Winsberg and Alexander.[73] Their analysis shows that the recoil range results for this reaction are consistent with compound-nucleus formation.

Agreement of the recoil angular distribution data with the calculations reinforces the conclusions about compound-nucleus formation, and further indicates that the compound system de-excites primarily by evaporation of neutrons having energy spectra similar to the form of Eq. (3.1). The agreement between the experimental and calculated distributions also suggests that there is no very great angular anisotropy in the neutron evaporation.

2. $Ra^{226}(\alpha, 4n)Th^{226}$

Figure 18 shows that the experimental recoil angular distributions agree quite well with the isotropic Monte Carlo

calculation with $E_\gamma = 0$ and $T = 1.0$ Mev. The value of T was obtained by Jackson fit to the excitation function of Vandenbosch.[78] The definition of the peak of the excitation function in this case allowed 0.2 to 0.3 Mev latitude in selection of the temperature. The value used here is comparable to the value of 0.9 Mev obtained by using the theoretical treatment of Cameron.[79]

The maximum experimental cross section for this reaction was reported by Vandenbosch to be about 500 mb.[78]

The recoil range data of Figure 21 and Table IV define a range-energy curve reasonably consistent with the theoretical expectations for this magnitude of recoil energy. The deviation of the recoil ranges below the theoretical values is consistent with the results reported by Valyocsik.[80] The approximate linearity of the data over the range of bombarding energy for which the reaction occurs is indicative of compound-nucleus formation.

Vandenbosch suggested that this reaction proceeds through a compound-nucleus mechanism based upon the magnitude of the experimental cross section. The recoil ranges and angular distributions appear to support this conclusion.

Of subsidiary interest here is the remarkably large range straggling of the Th^{226} recoils in hydrogen as compared with theory (Figure 19, Eq. 4.3, and Table IV). Harvey has shown that straggling of this magnitude could be caused by the momenta of the evaporated neutrons.[81] Valyocsik observed comparable range straggling in other recoil range measurements in gases.[80]

B. Reactions That Can Not be Fitted by the Simple Calculations

1. $Te^{130}(C^{12}, 5n)Ce^{137m}$

Figure 28 shows that the recoil ranges from the natural Te agree reasonably well with the ranges calculated from the Tb^{149} data. This is fairly convincing evidence for the formation of a compound nucleus. We suspect that the slight displacement of the points is caused by some systematic difference in experimental technique. If one neutron from the bombarding ion were to continue forward without transferring its momentum to the compound system, the energy loss

owing to the recoils produced would be less than 10%. It is possible that a consistent 10% decrease in the recoil ranges might be undetected in these experiments.

The slight sensitivity of the parameters T and B/A has already been discussed. The value of T = 2.5 Mev was selected by matching information on the experimental excitation function reported by Choppin;[4,5] this magnitude of temperature agrees reasonably with measured temperatures for neutrons emitted from heavy-ion reactions.[82] The value B/A = 1.2 was selected by using the semiclassical theory of Ericson and Strutinski.[63] This choice was in reasonable agreement with the experimental results of Knox[83] and Broek.[82] Since their experimental studies were made at much higher bombarding energies than used in this work, B/A = 1.2 is considered a maximum value. Figure 11 shows that if this value were reduced by a factor of 2 or 3, the angular distribution would broaden by about 0.3 degree.

Figure 25 shows that the recoil angular distributions diverge markedly from the calculated case for isotropic neutron emission and $E_\gamma = 0$. This indicates that a significant fraction of the excitation energy is being dissipated by some mechanism other than neutron emission. The magnitude of this difference greatly exceeds the most conservative estimates of error from all known sources. If the nonisotropic Monte Carlo calculation is used, with B/A and T fixed as already discussed, a fit to the experiments can be obtained by varying E_γ.

The values required to obtain fits are shown in Table VIII. They show a gradual increase with excitation energy. Use of E_γ in this way is equivalent to saying that the Q of the reaction is larger than its calculated ground-state value. If these Q values adjusted by E_γ are introduced into the Jackson calculation, the fit to the experimental excitation functions can be maintained by reducing T to about 2 Mev.

Figure 7 shows that a reduction in T by 0.5 Mev would cause the recoil angular distribution to become about 0.3 deg narrower; to compensate for this decrease, E_γ must also decrease by 1.5 Mev. On the other hand, if B/A should decrease to 0.1, there must be a compensating <u>increase</u> of E_γ by about 5 Mev.

The remarkable feature about the excitation-function data of Choppin and collaborators is that the maximum cross section occurs at an incident-particle energy which is 10 to 15 Mev higher than would be expected from simple theory, assuming an emission of neutrons with an average energy of 3 to 4 Mev. Huizenga[84] has pointed out that such neutron energies are to be expected.

The measured excitation functions were relative ones.[4, 5] The absolute values for the cross sections are not available.

A most interesting problem is to account for the differences between this reaction and the $Pr^{141}(C^{12}, 4n)$ reaction. In both cases the bombarding and excitation energies are comparable; their relationships to the closed shell at $N = 82$ differ slightly.

It is difficult to believe that the closed shell is responsible for the discrepancy in the excitation curves. Although it is known that closed shells appreciably alter the nuclear level structure, the closed shell in this case occurs 3 mass units from the product nuclide. At such a high level of excitation the density of accessible energy levels should be great enough for the statistical treatment to be valid.

In nuclear reactions induced by ions heavier than He^4, large quantities of angular momentum can be involved. In fact, angular-momentum effects in nuclear reactions have been a subject of great interest in the past several years.[5, 63-65, 82-95]

It would seem difficult to explain the differences in the particular cases described here on the basis of a statistical treatment of angular momentum effects, because of the comparable levels of bombarding energy and presumably comparable amounts of angular momentum transfer. Conceivably the observed effects might be due to the difference in the level structures of the target nuclei. This could be caused by even-odd effects.

In statistical treatments of nuclear reactions it has been usual to assume that the compound nucleus can de-excite most easily by neutron emission until the excitation energy is below the neutron binding energy.[60] It is then supposed that further de-excitation occurs by gamma emission. In this particular reaction the neutrons appear to carry away less energy than would be expected. A larger share of the de-excitation must occur by gamma emission. This effect has been

accounted for by the parameter E_γ. The enhanced gamma emission must be accompanied by some hindrance to neutron transitions. The role of angular momentum in this process is uncertain.

Possibly the combined effects of angular momentum and the closed shell could change the level density in such a way that the neutron transitions would be hindered.

One factor that has been ignored in this treatment is the competition from charged-particle emission. The possible effects of this competition are not known.

2. $Pb^{208}(\alpha, 2n)Po^{210}$

Figure 22 demonstrates that the experimental recoil angular distributions agree reasonably well with the calculations using T = 1.45 Mev up to a bombarding energy of about 28 Mev, which corresponds approximately to the maximum reaction cross section. At higher energies the experimental distributions become much more peaked forward than the calculations predict.

The maximum experimental cross section for this reaction was found by John to be 1.0 barn.[17]

The recoil-range data from natural Pb + He^4 shown in Figure 23 are very crude. For the magnitudes of recoil energies considered here, products from compound-nucleus processes are expected to have ranges approximately proportional to their energies. Such behavior is illustrated for the Bi(α, 2n) reaction in Figure 7 of Ref. 2. These lead experiments do not define a linear range-energy curve for compound-nucleus products; the dashed curve of Figure 23 was drawn rather arbitrarily. The major difficulties in making comparisons with the bismuth data were that, with the natural isotopic mixture of lead, each reaction produced several products which could not be conveniently removed from the thick targets for resolution by pulse-height analysis, as could be done in the bismuth experiments. Despite these obstacles, at about 28 Mev there is a reproducible departure from the trend of increasing recoil range with increasing bombarding energy. Although the points are displaced compared with the bismuth data of Ref. 2, there is a great similarity in the behavior of the recoil ranges for the high-energy side of the

(α, 2n) excitation function. This levelling off in the recoil-range curve occurs in the energy range in which the observed product activities are predominantly Po^{208} and Po^{210} from (α, 2n) reactions.

This evidence from both types of experiments indicates that, beginning at a bombarding energy of about 28 Mev, this reaction proceeds with approximately 10% to 20% of some mechanism other than compound-nucleus formation; the fraction of direct mechanism is estimated from the departure of the recoil ranges and angular distributions from the predicted compound-nucleus case. This would correspond to a 100- to 200-mb cross section for such a mechanism. The direct mechanism might cause the incident alpha particle either to knock a neutron out of the target nucleus or to be "stripped" of one neutron upon entering the nucleus; further de-excitation could then occur through evaporation of a second neutron.

No attempt was made to fit the Monte Carlo calculations by assigning values to E_γ. For such a large contribution from direct processes, the assumptions about the neutron energy spectrum would be questionable.

The experimental results presented here are very similar to the results obtained by Harvey et al. for $Bi^{209}(\alpha, 2n)At^{211}$;[2] however, in this work the recoil angular distributions appear to differ drastically from the calculated ones.

Brown and Muirhead[96] had some success in fitting the experimental Bi+n neutron angular distribution data of Rosen and Stewart[97] by use of a nuclear cascade calculation, assuming that the mean free path for the incident neutron in a nuclear Fermi well was of approximately nuclear dimensions. Application of such a calculation to these (α, 2n) reactions was considered; however, it was believed that the assumptions about the mean free path were less appropriate for an alpha-particle reaction.

The idea of a surface reaction mechanism is slightly more attractive.[98] This classification includes so-called "optical-type" and "stripping" reactions. An (α, 2n) reaction is equivalent to bringing a pair of protons into a nucleus. For the $Pb^{208}(\alpha, 2n)Po^{210}$ reaction treated here and the $Bi^{209}(\alpha, 2n)At^{211}$ reaction studied by Harvey[2], both the target and product nuclei lie on the N = 126 closed shell;

Pb^{208} is also located at the Z = 82 shell closure. The abnormally large spacing of the neutron resonance levels in Pb^{208} has been known for some time.[99] This location on the closed shells could lead to the expectation of having fair "purity" of shell-model states just outside the closed shells. The criterion that has been given for the enhanced probability for surface interactions is a "similarity" in the configurations of the initial and final states.[98] In these particular reactions that requirement might be achieved. Other evidence has been cited for similarities between nuclei which differ by a pair of nucleons.[100]

It is difficult to reconcile a 100- to 200-mb cross section for a direct mechanism to theories for direct interactions. Serber's theoretical treatment of deuteron stripping, well supported by experiments, predicted a deuteron-stripping cross section for heavy elements of about 300 mb;[101] the α particle, being much more tightly bound than a deuteron, should be more difficult to break apart. Silva's experiments with α-particle stripping reactions of Bi^{209} gave an (α, d) cross section of 2 to 3 mb and an (α, pn) cross section of 18 to 20 mb.[102] The largest of these cross sections is less by a factor of 5 to 10 than would give agreement with the (α, 2n) results.

Additional interesting information about this type of reaction would probably be obtained by applying these techniques to other (α, 2n) reactions, particularly those involving nuclei away from closed shells.

3. $Pb^{207}(\alpha, n)Po^{210}$

Figure 24 shows the poor agreement between typical experimental and calculated recoil angular distributions for this reaction. John's experimental excitation function[17] does not permit a precise choice of nuclear temperature by the Jackson procedure; however, the experiments disagreed in the same way with calculations using T = 0.5, 1.4, and 2.0 Mev. In almost every case the maximum in the experimental curve occurred at a much smaller angle than in the calculated case.

The maximum cross section for this reaction was reported by John to be about 100 mb.[17]

The disagreement between the experiments and calculations is probable evidence that the reaction occurs to a large extent through some

direct-interaction mechanism. The shift in the maximum in the recoil angular distributions to smaller angles would be consistent with such a mechanism.

Another possible reason for the disagreement is that the excitation energy in the (α, n) reaction could be insufficient to justify application of a statistical treatment.

VI. CONCLUDING REMARKS

From these studies it is concluded that the experimental techniques described here are useful for obtaining information about certain features of nuclear reactions involving the emission of several neutrons.

The method for calculating the recoil angular distributions by Monte Carlo methods appears to be useful for detecting major departures from the simple compound-nucleus-statistical-evaporation model; however, where there is substantial competition from reaction mechanisms other than neutron evaporation, interpretation of the results becomes uncertain.

It is particularly interesting that agreement between experiments and calculations has not been achieved for He^4-induced reactions involving evaporation of less than three neutrons.[1, 2] So far, all such reactions examined were complicated by the proximity of closed shells. It is possible that closed-shell effects might reduce the validity of the statistical approach; therefore, better agreement with the calculations might be expected with nuclei located away from closed shells.

ACKNOWLEDGMENTS

I wish to thank Professor John O. Rasmussen for his interest and encouragement during the course of this work.

I am particularly grateful to Dr. Bernard G. Harvey for his guidance and interest.

The assistance and many helpful suggestions from Dr. Paul F. Donovan and Ernest W. Valyocsik during the early stages of this investigation are greatly appreciated.

I am very grateful to Dr. John M. Alexander and Professor Gregory R. Choppin (currently at Florida State University) for many helpful suggestions, for assistance with experiments, and for allowing me access to their experimental results prior to publication.

I wish to thank Joseph Cerny, Jack Elliott, Richard Pehl, and Leon Petrakis for assistance with several of the experiments.

I deeply appreciate the helpful discussions with Dr. John R. Huizenga, Dr. W. J. Knox, Dr. Lester Winsberg, Dr. Jose Gonzalez-Vidal, Dr. Glen E. Gordon, Dr. H. Marshall Blann, James F. Mollenauer, and Jonas Alster.

The assistance of the operating staffs of the HILAC and the 60-inch cyclotron deserves very special mention.

For their valuable assistance in the preparation of many of the targets, I wish also to thank Dan O'Connell and his staff.

I appreciate the assistance given to me by Walter Hutchinson and Douglas Brainard of the Computer Group.

I gratefully acknowledge the assistance of the Analytical and Optical Spectroscopy Groups for their help with the chemical analyses.

The assistance of the Health Chemistry Group given during this work is greatly appreciated.

I wish to thank my wife, Mary Lou, for her patience and understanding during this work and for typing many early drafts of this thesis.

This work was performed under the auspices of the United States Atomic Energy Commission

APPENDICES

A. FORTRAN Program Listing for Isotropic Monte Carlo Calculation

The data used for the calculations were organized on data cards in the following way. (The data cards as described here also apply to Appendix B. The cards are interchangeable between the programs.)

Card 1	Month, day, year--2 digits each.
Card 2	R(I)--radii of catcher rings (cm).
Card 3	MOFP, ZOFP, MOFT, ZOFT--mass and charge numbers of projectile and target.
Card 4	T--Nuclear temperature (Mev).
	D--Target-catcher distance (cm).
	NRXN--number of neutrons evaporated in this reaction.
	REX = E_γ (Mev).
	F, G } Same as A and B in neutron angular distribution (these numbers are read but not used in the isotropic calculation).
	NS--Parameter to determine number of each kind of reaction occurring; when zero, the number of reactions occurring up to (x + 1)n is recorded.
Card 5	Q(I)--Reaction Q's from (ion, n) to [ion, (x+1)n].
Card 6	ELAB--Bombarding energy (Mev).
	N--Number of cases to be run.

```
 4 FORMAT(66H                                    MONTE CARLO CALCULATION FO
  XR MOFP =   I2,9H  ZOFP = I2,9H  MOFT = I3,9H  ZOFT = I3///)
 6 FORMAT(2H1 I2,2H /,I2,2H /I2/)
 8 FORMAT(3I10)
 9 READ8,MONTH,DAY,YEAR
11 READ 21,(R(I),I=1,11)
12 FORMAT(4I10)
14 READ12,MOFP,ZOFP,MOFT,ZOFT
10 PRINT6,MONTH,DAY,YEAR
16 PRINT4,MOFP,ZOFP,MOFT,ZOFT
18 FORMAT(2F10.2,I10,F10.2,2E10.4,I10)
19 FORMAT(28X7H REX = F8.2,10X5H T = F8.2//)
20 READ18,T,D,NRXN,REX,F,G,NS
21 FORMAT(11F6.3)
22 FORMAT(13F10.2)
23 PRINT 19, REX, T
24 DIMENSION Q(13), EX(13), PHI(11), SAC(11), EN(13), V(12), P(12)
25 DIMENSION R(11),AA(11),BB(11),PSI(11),ENSUM(13),Z(2049),NA(12)
26 M = NRXN + NS + 1
27 READ 22,(Q(I), I=1,M)
28 FORMAT(F10.2,I10)
29 FORMAT(47H                                          ELAB = F8.2//)
30 READ28,ELAB,N
31 PRINT 29,ELAB
32 AOFT = MOFT
34 AOFP = MOFP
36 ECM = ((ELAB*AOFT)/(AOFT+AOFP)) - REX
37 PA = SQRTF(2.*AOFP*(ECM + REX))
39 DO 40 I=1,M
```

```
 40 EX(I) = ECM + Q(I)
 41 ENSUM(1) = 0.
 45 ENN = N
 47 FORMAT (9H SUMAA = F10.1)
 52 DO 54 I=1,11
 54 PHI(I)= ATANF( R(I)/D)
 57 SAC(1) =1.
 58 DO  60 I=2,11
 60 SAC(I)=(1.-COSF(PHI(1)))/(COSF(PHI(I-1))-COSF(PHI(I)))
 71 FORMAT(5H Q = 13F8.2///)
 73 PRINT 71,(Q(I), I=1,M)
 74 DO 75 I=1,11
 75 AA(I) = 0.
204 DELTAE = EX(1)/2048.
206 Z(1) = 1.
207 DO 210 N=2,2049
208 E = N-1
209 PAR = (E*DELTAE)/T
210 Z(N) = EXPF(-PAR)*(1.+PAR)
 78 FORMAT(5H N = 13F8.5)
 79 FORMAT(5H J = I5,7H ZEX = F8.5,6H ZR = F8.5,6H FN = F7.1)
 80 DO 81 I=1,M
 81 NA(I) = 0
 83 SUMAA = 0.
 86 DO 102 I=1,M
214 J = (EX(I)-ENSUM(I))/DELTAE
216 N = J+1
218 ZEX = Z(N)
220 ZR = (RANF(X))*(1.-ZEX)+ZEX
221 CALL SCAN (ZR,Z,FN)
```

```
224 EN(I) = (FN*DELTAE)-DELTAE
 92 IF(SENSE SWITCH 2)94,95
 94 PRINT 78,(EN(K), K=1,M )
    PRINT 79,J,ZEX,ZR,FN
 95 ENSUM(I+1) = EN(I) + ENSUM(I)
 96 IF(EX(I+1) - ENSUM(I+1))97,97,101
 97 NA(I) = NA(I) + 1
 99 GO TO 103
101 IF(I-13 ) 102,83,83
102 CONTINUE
103 IF(NRXN-I )83,105,83
105 DO 106 I=1,NRXN
106 P(I) = SQRTF(2.*EN(I))
107 V(1) = P(1)
108 IF(I-1 )120,120,110
110 DO 118 I = 2,NRXN
114 RN = 2.*RANF(X) - 1.
116 V(I) = SQRTF((V(I-1))**2 +(P(I))**2 +2.*V(I-1)*P(I)*RN)
117 IF(I-NRXN) 118,120,120
118 CONTINUE
120 RN = 2.*RANF(X) - 1.
124 THETA = ATANF((SQRTF(1.-RN**2))/(RN+PA/V(I)))
126 DO 130 I=1,11
128 IF(THETA - PHI(I)) 132,132,129
129 IF(I-11) 130,132,132
130 CONTINUE
132 AA(I) = AA(I) + 1.
421 DO 422 I=1,11
422 SUMAA = SUMAA + AA(I)
423 IF(SENSE SWITCH 3) 424,425
```

```
424 PRINT 47, SUMAA
425 IF(SENSE SWITCH 4) 428,426
426 IF(ENN - SUMAA) 428,428,83
428 DO 429 I=1,11
429 BB(I)=AA(I)*SAC(I)
430 PSI(1)=57.296*PHI(1)/2.
431 DO 432 I=2,11
432 PSI(I) = 28.648*(PHI(I-1)+PHI(I))
435 FORMAT(110H    PSI(1)    PSI(2)    PSI(3)    PSI(4)    PSI(5)    P
   XSI(6)    PSI(7)    PSI(8)    PSI(9)    PSI(10)    PSI(11))
436 PRINT 435
437 FORMAT (11F10.3//)
438 PRINT 437, (PSI(I), I=1,11)
440 PRINT 437,(BB(I),I=1,11)
444 FORMAT(107H      N1       N2       N3       N4       N5       N6
   X     N7       N8       N9       N10      N11      N12  //)
446 PRINT 444
448 FORMAT (12I9  ///)
450 PRINT 448, (NA(I),I=1,M)
451 IF(SENSE SWITCH 1)453,452
452 GO TO 30
453 GO TO 14
456 END(0,1,0,0,0)
```

B. FORTRAN Program Listing for Nonisotropic Monte Carlo Calculation

(See Appendix A for summary of data cards)

```
 4 FORMAT(66H                                    MONTE CARLO CALCULATION FO
  XR MOFP =  I2,9H  ZOFP = I2,9H  MOFT = I3,9H  ZOFT = I3///)
 6 FORMAT(2H1 I2,2H /,I2,2H /I2/)
 8 FORMAT(3I10)
 9 READ8,MONTH,DAY,YEAR
11 READ 21,(R(I),I=1,11)
12 FORMAT(4I10)
14 READ12,MOFP,ZOFP,MOFT,ZOFT
10 PRINT6,MONTH,DAY,YEAR
16 PRINT4,MOFP,ZOFP,MOFT,ZOFT
18 FORMAT(2F10.2,I10,F10.2,2E10.4,I10)
19 FORMAT(28X7H REX = F8.2,10X5H T = F8.2/28X5H F = E10.4,8X5H G = E1
  X0.4//)
20 READ18,T,D,NRXN,REX,F,G,NS
21 FORMAT(11F6.3)
22 FORMAT(13F10.2)
23 PRINT 19, REX, T,F,G
24 DIMENSION Q(13), EX(13), PHI(11), SAC(11), EN(13),        P(12)
25 DIMENSION R(11),AA(11),BB(11),PSI(11),ENSUM(13),Z(2049),NA(12)
   DIMENSION CHI(12),TN(10),            ANGLE(10), W(2049)
   DIMENSION  SACA(10), TAN(10)
26 M = NRXN + NS + 1
27 READ 22,(Q(I), I=1,M)
28 FORMAT(F10.2,I10)
29 FORMAT(47H                                          ELAB = F8.2//)
30 READ28,ELAB,N
31 PRINT 29,ELAB
32 AOFT = MOFT
34 AOFP = MOFP
```

```
 36 ECM = ((ELAB*AOFT)/(AOFT+AOFP)) - REX
 37 PA = SQRTF(2.*AOFP*(ECM + REX))
 39 DO 40 I=1,M
 40 EX(I) = ECM + Q(I)
 41 ENSUM(1) = 0.
 45 ENN = N
 47 FORMAT (9H SUMAA = F10.1)
 52 DO 54 I=1,11
 54 PHI(I)= ATANF( R(I)/D)
 57 SAC(1) =1.
 58 DO  60 I=2,11
 60 SAC(I)=(1.-COSF(PHI(1)))/(COSF(PHI(I-1))-COSF(PHI(I)))
 71 FORMAT(5H Q = 13F8.2///)
 73 PRINT 71,(Q(I), I=1,M)
 74 DO 75 I=1,11
 75 AA(I) = 0.
204 DELTAE = EX(1)/2048.
206 Z(1) = 1.
207 DO 210 N=2,2049
208 E = N-1
209 PAR = (E*DELTAE)/T
210 Z(N) = EXPF(-PAR)*(1.+PAR)
150 DELCHI = 3.14159/2048.
151 W(1) = 2. *(F + G/3.)
152 TRM = W(1)/2.
153 DO 156 N = 2,2049
154 GE = N - 1
155 ANG = GE * DELCHI
156 W(N) = F * COSF(ANG) + G/3.* (COSF(ANG))**3 + TRM
550 DO 554 N = 1,10
```

```
 82 TN(N) = 0.
552 B = N
554 ANGLE(N) = B*.314159
400 SACA(1) = 1.
402 DO 404 I = 2,10
404 SACA(I)=(1.-COSF(ANGLE(1)))/(COSF(ANGLE(I-1))-COSF(ANGLE(I)))
650 IF(SENSE SWITCH 1) 652,80
    DIMENSION SE(65), NN(65,12)
652 DO 656 J =1,65
654 DO 656 I=1,NRXN
656 NN(J,I) = 0
658 DELN = 0.20
660 DO 664 J=2,65
662 FT = J - 1
664 SE(J) = FT* DELN
666 SE(1) = 0.
 80 DO 81 I=1,M
 81 NA(I) = 0
 83 SUMAA = 0.
 86 DO 102 I=1,M
214 J = (EX(I)-ENSUM(I))/DELTAE
216 N = J+1
218 ZEX = Z(N)
220 ZR = (RANF(X))*(1.-ZEX)+ZEX
221 CALL SCAN (ZR,Z,FN)
224 EN(I) = (FN*DELTAE)-DELTAE
 95 ENSUM(I+1) = EN(I) + ENSUM(I)
 96 IF(EX(I+1) - ENSUM(I+1))97,97,101
 97 NA(I) = NA(I) + 1
 99 GO TO 103
```

```
101 IF(I-13 ) 102,83,83
102 CONTINUE
103 IF(NRXN-I )83,105,83
105 DO 106 I=1,NRXN
106 P(I) = SQRTF(2.*EN(I))
670 IF(SENSE SWITCH 1) 672,499
672 DO 676 I=1,NRXN
674 CALL LOOKUP (EN,SE,J, I)
676 NN(J,I) = NN(J,I) + 1
499 PX = 0.
500 PY = 0.
501 PZ = 0.
502 DO 528 I=1,NRXN
503 WR = W(1) * RANF(X)
504 CALL SCAN (WR, W, FN)
505 CHI(I) = (FN * DELCHI) - DELCHI
108 IF (SENSE SWITCH 5) 110,512
110 DO 116 N=1,10
112 IF (CHI(I) - ANGLE(N)) 118,118,114
114 IF(N-10) 116,118,118
116 CONTINUE
118 TN(N) = TN(N) + 1.
512 IF(I-1) 514,514,520
514 CHIR = COSF(CHI(I))
515 V = P(1)
516 IF(NRXN - 1) 531,531,520
520 RAZIM = 6.2831854 * RANF(X)
521 PX = PX + P(I) * SINF(CHI(I)) * COSF(RAZIM)
522 PY = PY + P(I) * SINF(CHI(I)) * SINF(RAZIM)
523 PZ = PZ + P(I) * COSF(CHI(I))
```

```
526 IF(I-NRXN) 528,529,529
528 CONTINUE
529 V = SQRTF(PX**2 + PY**2 + PZ**2)
530 CHIR = PZ/V
531 THETA = ATANF((SQRTF(1. - CHIR**2))/(CHIR + PA/V))
126 DO 130 I=1,11
128 IF(THETA - PHI(I)) 132,132,129
129 IF(I-11) 130,132,132
130 CONTINUE
132 AA(I) = AA(I) + 1.
421 DO 422 I=1,11
422 SUMAA = SUMAA + AA(I)
423 IF(SENSE SWITCH 3) 424,425
424 PRINT 47, SUMAA
425 IF(SENSE SWITCH 4) 428,426
426 IF(ENN - SUMAA) 428,428,83
428 DO 429 I=1,11
429 BB(I)=AA(I)*SAC(I)
430 PSI(1)=57.296*PHI(1)/2.
431 DO 432 I=2,11
432 PSI(I) = 28.648*(PHI(I-1)+PHI(I))
435 FORMAT(110H     PSI(1)     PSI(2)     PSI(3)     PSI(4)     PSI(5)     P
   XSI(6)     PSI(7)     PSI(8)     PSI(9)    PSI(10)    PSI(11))
436 PRINT 435
437 FORMAT (11F10.3//)
438 PRINT 437, (PSI(I), I=1,11)
440 PRINT 437,(BB(I),I=1,11)
444 FORMAT(107H       N1        N2        N3        N4        N5        N6
   X      N7        N8        N9       N10       N11       N12  //)
445 FORMAT (1X 10E11.3///)
```

```
446 PRINT 444
447 FORMAT (1X10F11.5//)
448 FORMAT (12I9  ///)
449 FORMAT(26H NEUTRON ANGULAR SPECTRUM /7X3H A1,8X3H A2,8X6H A3,8X3H
   XA4,8X3H A5,8X3H A6,8X3H A7,8X3H A8,8X3H A9,8X4H A10 )
450 PRINT 448, (NA(I),I=1,M)
570 IF (SENSE SWITCH 5) 572,453
572 PRINT 449
574 PRINT 447, (ANGLE(N), N=1,10)
408 DO 410 I = 1,10
    N = I
410 TAN(I) = TN(N)*SACA(I)
576 PRINT 445, (TAN(I), I=1,10)
680 IF(SENSE SWITCH 1) 682,453
682 PRINT 690
684 DO 688 J=1,65
688 PRINT 692, SE(J),(NN(J,I), I=1,NRXN)
690 FORMAT(24H NEUTRON ENERGY SPECTRA  /8H ENERGY 5X4H N1 4X4H N2 4X4H
   X N3 4X4H N4 4X4H N5 4X4H N6 4X4H N7 4X4H N8 4X4H N9 4X5H N10 4X5H
   XN11 4X5H N12 //)
692 FORMAT (F6.1, 2X12I8)
453 GO TO 14
456 END (0,1,0,0,0)
```

C. FORTRAN Program Subroutines for the Monte Carlo Calculations

Subroutine SCAN searches the 2049-space tables of Z and R. Subroutine LOOKUP locates the neutron energies in the neutron energy spectra.

```
300 SUBROUTINE SCAN (ZR,Z,FN)
    DIMENSION Z(2049)
301 N = 1025
302 IF(ZR-Z(N))303,222,305
303 N=N+512
304 GO TO 307
305 N=N-512
306 GO TO 307
307 IF(ZR-Z(N))308,222,310
308 N=N+256
309 GO TO 312
310 N=N-256
311 GO TO 312
312 IF(ZR-Z(N))313,222,315
313 N=N+128
314 GO TO 317
315 N=N-128
316 GO TO 317
317 IF(ZR-Z(N))318,222,320
318 N=N+64
319 GO TO 322
320 N=N-64
321 GO TO 322
322 IF(ZR-Z(N))323,222,325
323 N=N+32
324 GO TO 327
325 N=N-32
326 GO TO 327
327 IF(ZR-Z(N))328,222,330
```

```
328 N=N+16
329 GO TO 332
330 N=N-16
331 GO TO 332
332 IF(ZR-Z(N))333,222,335
333 N=N+8
334 GO TO 337
335 N=N-8
336 GO TO 337
337 IF(ZR-Z(N))338,222,340
338 N=N+4
339 GO TO 342
340 N=N-4
341 GO TO 342
342 IF(ZR-Z(N))343,222,345
343 N=N+2
344 GO TO 347
345 N=N-2
346 GO TO 347
347 IF(ZR-Z(N))348,222,350
348 N=N+1
349 GO TO 226
350 N=N-1
351 GO TO 226
226 IF(ZR-Z(N)) 222,222,228
228 N = N + 1
222 FN = N
223 RETURN
352 END (0,1,0,0,1)
```

```
600 SUBROUTINE LOOKUP (EN, SE, J, I)
    DIMENSION EN(13) , SE(65)
601 J = 33
602 IF(EN(I) - SE(J)) 605, 627, 603
603 J = J + 16
604 GO TO 607
605 J = J - 16
606 GO TO 607
607 IF(EN(I) - SE(J)) 610,627,608
608 J = J + 8
609 GO TO 612
610 J = J - 8
611 GO TO 612
612 IF(EN(I) - SE(J)) 615,627,613
613 J = J + 4
614 GO TO 617
615 J = J - 4
616 GO TO 617
617 IF(EN(I) - SE(J)) 620,627,618
618 J = J + 2
619 GO TO 622
620 J = J - 2
621 GO TO 622
622 IF(EN(I) - SE(J)) 625,627,623
623 J = J + 1
624 GO TO 629
625 J = J - 1
626 GO TO 629
```

```
629 IF(EN(I)-SE(J)) 627,627,630
630 J = J + 1
627 RETURN
628 END(0,1,0,0,0)
```

D. Derivations of the Integral Probability Functions Used in the Calculations

1. Derivation of the integral energy probability function

In Sec.III-1 we assume the neutron-energy spectrum to have the form

$$P(E_n) = \frac{dn}{dE_n} = E_n \exp(-E_n/T). \qquad \text{(D-1)}$$

Integrating gives

$$n = -T^2 \exp(-E_n/T) \left(\frac{E_n}{T} + 1\right) + C. \qquad \text{(D-2)}$$

Then, applying the boundary conditions:

(a) $n = 0$ for $E_n/T = 0$,

and $0 = -T^2 + C$, $C = T^2$;

(b) $n = 1$ for $E_n/T = 10$,

and $1 = T^2 [1 - e^{-10} (11)] \approx T^2$;

and substituting in (D-2):

$$n = 1 - \exp(-E_n/T) \left(\frac{E_n}{T} + 1\right). \qquad \text{(D-3)}$$

The distribution is then inverted by defining

$$Z = 1-n = \exp(-E_n/T) \left(\frac{E_n}{T} + 1\right), \qquad \text{(D-4)}$$

which is the energy probability function illustrated in Figure 9.

2. Derivation of the angular probability function

We wish to have anistropy with the form

$$W(\theta) = \frac{dR}{d\Omega} = A + B \cos^2\theta, \qquad \text{(D-5)}$$

where $dR = (A + B \cos^2\theta)\, d\Omega$; but $d\Omega = 2\pi \sin\theta d\theta$,

so $dR = 2\pi \sin\theta\, (A + B \cos^2\theta)\, d\theta$.

Integrating this from 0 to π and absorbing 2π into the constants gives

$$R = A \cos\theta + \frac{B}{3} \cos^3\theta, \qquad \text{(D-6)}$$

for $G \to 0$, $R \to A \cos\theta$, the condition for isotropy; and for $G \to \infty$, $R \to \frac{B}{3} \cos^3\theta$. The limits are, for $\theta = 0$, $R = A + \frac{B}{3}$,

and for $\theta = \pi$, $R = -(A + \frac{B}{3})$.

To eliminate the need for changing the sign of R for second-quadrant angles, the function is adjusted by shifting the ordinate to allow all values of R to be positive, hence

$$R = (A \cos\theta + \frac{B}{3} \cos^3\theta) + A + \frac{B}{3}, \qquad \text{(D-7)}$$

which is the energy probability function illustrated in Figure 12.

APPENDIX E

A summary of the recoil angular distributions calculated by the Monte Carlo method follows in Tables E-I through E-V.

TABLE E-I

Summary of Monte Carlo recoil angular distribution data — $Ra^{226}(\alpha, 4n)Th^{226}$, T = 1.0 Mev

E_α Mev	Relative $d\sigma/d\Omega$, for angles in degrees[a]											W(1/2)[c] Degrees
	2.31	5.97	8.72	11.47	14.24	16.88	19.37	21.85	24.23	26.57	28.75	
32.9[b]	850	529	263	84.1	8.00	0						7.0
34.1	1319	957	572	240	64.2	6.64	0					8.6
35.5	1114	817	540	302	116	30.8	4.40	0				8.2
36.1	1100	790	543	294	127	37.4	6.38	0				8.3
37.2	925	760	549	314	143	49.7	13.9	1.27	0.19	0		9.5
38.2	890	768	512	318	151	62.9	16.3	1.90	0			9.4
39.3	906	733	514	298	159	65.6	25.1	4.64	0.38	0		9.2
40.2	865	728	528	286	159	70.1	24.6	8.44	3.05	0		9.8
41.6	853	723	489	308	156	74.1	32.8	8.87	1.90	1.29	0	9.3
42.2	839	687	499	300	168	81.8	30.4	9.29	3.05	0.37	0	9.5
43.2	752	668	478	302	192	82.8	39.6	11.8	5.71	0.37	0.19	10.0
44.5	737	620	477	317	187	94.0	40.9	15.0	4.95	1.29	0	10.3
46.2	656	535	460	330	188	116	56.8	23.6	5.71	1.11	0.56	11.3

[a] See reference 69.

[b] 2568 cases for 32.9 Mev; all others, 5000 cases.

[c] Overall error estimated to be $< \pm 0.5$ degrees.

TABLE E-II

Summary of Monte Carlo recoil angular distribution data – $Pb^{208}(\alpha, 2n)Po^{210}$, T = 1.45 Mev

E_α Mev	Relative $d\sigma/d\Omega$, for angles in degrees[a]										$W(1/2)$[b] Degrees
	2.31	5.97	8.72	11.47	14.24	16.88	19.38	21.85	24.23	26.57	
21.7	1642	1272	597	36.3	0						7.7
22.3	1339	1114	684	154	1.06	0					8.8
23.1	1130	926	657	304	33.6	0					9.2
24.0	974	830	606	359	96.2	5.04	0				10.0
25.1	878	759	570	345	160	26.6	0.44	0			10.0
26.2	886	726	535	337	172	53.1	5.06	0			10.0
27.2	849	706	506	322	188	64.5	16.5	0			9.8
28.7	816	691	508	315	181	80.2	22.9	2.11	0		10.2
29.7[c]	493	432	330	208	116	45.9	13.9	2.53	0.19	0	10.6
31.7	666	616	488	348	202	87.9	36.8	10.5	0.76	0	11.0
33.0	615	525	455	341	232	129	36.3	13.1	0.76	0	12.5
35.2	498	478	386	316	241	173	69.1	23.9	4.00	0.18	14.0
37.2	464	376	383	315	223	166	114	37.6	6.28	1.48	14.2

[a] See reference 69.

[b] Overall error is estimated to be < ± 0.5 degree.

[c] Case for 29.7 Mev was 3168 cases; all others were 5000 cases.

TABLE E-III

Summary of Monte Carlo recoil angular distribution data[a] — $Pb^{207}(\alpha, n)Po^{210}$

E_α Mev	Relative $d\sigma/d\Omega$, for angles in degrees[b]										
	1.54	3.99	5.84	7.70	9.61	11.44	13.20	14.97	16.71	18.44	20.09
T = 0.5 Mev											
19.7	1219	1022	565	230	53.6	9.91	1.61	0			
20.5	998	1089	618	227	58.1	7.68	1.81	0			
21.7[c]	304	342	414	600	196	33.4	2.81	0.56	0.16	0	
22.3[d]	90	110	114	159	148	26.5	3.61	0.38	0		
T = 2.00 Mev											
19.7	350	345	357	278	228	159	104	56.5	19.4	0.31	0
20.5	332	357	356	284	223	154	99.7	54.8	25.9	2.94	0
21.7	218	209	246	319	261	178	120	58.9	36.1	11.3	0
22.3	169	170	194	271	298	208	125	70.9	36.2	13.8	0.15
23.1	154	153	172	198	269	236	160	78.8	44.5	19.0	1.82
24.0	113	135	135	162	185	280	195	106	56.2	19.7	4.70
T = 1.40 Mev											
19.7	456	457	408	325	224	125	68.8	30.4	9.72	0.16	0
21.7	237	246	280	423	298	163	76.5	34.0	13.5	3.56	0
20.5	421	498	416	321	219	128	66.0	27.4	9.06	2.17	0

-continued next page-

TABLE E-III (continued)

E_α Mev	T = 1.40 Mev: Relative $d\sigma/d\Omega$, for angles in degrees[e] 2.32	5.97	8.72	11.47	14.24	16.88	19.38	21.85
22.3	434	543	802	438	138	35.0	5.50	0
23.1	358	446	579	604	193	48.3	4.40	0
24.0	305	345	431	661	268	67.2	10.3	0

[a] These data represent 5000 cases except where indicated.

[b] See reference 70.

[c] 4478 cases.

[d] 1700 cases.

[e] See reference 69.

TABLE E-IV

Summary of Monte Carlo recoil angular distribution data[a] — $Pr^{141}(C^{12}, 4n)Tb^{149}$, T = 1.5 Mev

$E_{C^{12}}$	Relative $d\sigma/d\Omega$, for angles in degrees[b]										W(1/2)[c]
Mev	1.54	3.99	5.84	7.70	9.61	11.44	13.20	14.97	16.71	18.44	Degrees
55.0	1425	898	405	89.6	6.64	0					4.2
58.0	1098	816	434	176	35.8	2.97	0				5.0
61.5	965	724	446	207	68.8	8.42	0				5.5
64.5	919	710	420	219	72.8	23.0	3.21	0.19	0		5.5
69.5	820	603	404	238	111	36.2	8.83	1.69	0		5.7
71.5	693	604	410	250	118	45.8	10.4	2.06	0		6.4
75.0	683	506	391	252	141	57.0	21.0	2.82	0.33	0	6.3

[a] 4000 cases for each energy.

[b] See reference 70.

[c] Overall error is estimated to be $< \pm 0.5$ degree.

TABLE E-V

Summary of Monte Carlo recoil angular distribution data — $Te^{130}(C^{12}, 4n)Ce^{137}$

$E_{C^{12}}$ Mev	No. Cases	Relative $d\sigma/d\Omega$, for angles in degrees[a] 1.54	3.99	5.84	7.70	9.61	11.44	13.20	14.97	16.71	W(1/2)[b] Degrees
T = 2.5 Mev, B/A = 1.2											
59.0	2023	681	394	208	70.4	13.7	1.98	0			4.2
64.5	4819	1215	850	516	245	86.3	15.6	1.40	0		5.3
69.0	7018	1579	1122	744	399	153	48.8	10.6	0.56	0	5.4
75.0	2000	383	319	196	123	53.8	19.1	5.42	1.13	0	5.7
81.0	8641	1616	1256	907	515	241	91.6	30.7	6.94	0.99	6.1
87.5	9652	1762	1415	977	579	294	107	30.3	8.26	0.82	6.3
T = 1.5 Mev, B/A = 1.2											
59.0	10000	3250	2086	993	344	69.8	6.93	0.20	0		4.7
64.5	10000	2641	1870	1045	490	137	30.0	5.02	0.38		5.2
69.0	9716	2479	1750	1040	470	160	36.2	7.63	0.56	0	5.7
75.0	7237	1548	1206	735	398	168	62.4	14.4	3.00	0.33	5.7
81.0	10000	1798	1486	992	599	303	117	37.7	7.69	1.65	6.2
87.5	3580	670	521	330	204	111	49.3	17.9	5.63	0.66	5.7

-continued next page-

TABLE E-V (continued)

T = 2.5 Mev, isotropic											
$E_{C^{12}}$ Mev	No. Cases	Relative $d\sigma/d\Omega$, for angles in degrees[a]									W(1/2)[b] Degrees
		1.54	3.99	5.84	7.70	9.61	11.44	13.20	14.97	16.71	
59.0	2000	389	289	221	117	54.3	20.1	4.42	0.75	0	6.2
64.5	2000	323	235	204	133	62.4	30.0	13.0	4.50	0.66	6.6
69.0	2000	270	192	126	74.1	37.1	13.6	5.44	1.15	0.31	7.5
75.0	2000	239	210	170	126	82.0	45.8	20.7	8.44	2.64	7.6
81.0	2000	218	187	164	112	82.0	52.5	27.9	14.1	5.76	8.7
87.5	2000	177	184	148	107	86.0	55.7	33.1	19.3	6.42	8.7

[a] See reference 70.

[b] Overall error is estimated to be < ± 0.5 degree.

REFERENCES

1. P. F. Donovan, B. G. Harvey, and W. H. Wade, Phys. Rev. 119, 218 (1960).

2. B. G. Harvey, W. H. Wade, and P. F. Donovan, Phys. Rev. 119, 225 (1960).

3. B. G. Harvey, in Annual Reviews of Nuclear Sciences, Vol. 10, E. Segrè, Ed. (Annual Reviews, Inc., Palo Alto, Calif., 1960), p. 235. The bibliography of this review article contains many general references to recent recoil studies not repeated here.

4. G. R. Choppin and T. Klingen, Florida State University, Tallahassee, Florida (unpublished data).

5. G. R. Choppin, Research in Nuclear Chemistry, Progress Report, June 1, 1959 - May 31, 1960, Florida State University, Tallahassee, Florida (unpublished).

6. Oak Ridge National Laboratory enriched isotope sample analysis.

7. E. B. Sandell, Colorimetric Determination of Traces of Metals, (Interscience Publishers, New York, 1959).

8. W. A. Aron, B. G. Hoffman, and F. C. Williams, Range-Energy Curves, Rev. ed., USAEC Report AECU-663 (UCRL-121), May 28, 1951.

9. J. R. Walton, Lawrence Radiation Laboratory, Berkeley (unpublished data).

10. L. C. Northcliffe, Phys. Rev. 120, 1744 (1960).

11. This Q value was calculated from the atomic masses tabulated in B. M. Foreman, Jr., and G. T. Seaborg, J. Inorg. and Nuclear Chem. 7, 305 (1958).

12. M. H. Studier and E. K. Hyde, Phys. Rev. 74, 591 (1948).

13. G. von Dardel, Phys. Rev. 79, 734 (1950).

14. P. C. Marin, Brit. J. Appl. Phys. 7, 188 (1956).

15. D. Strominger, J. M. Hollander, and G. T. Seaborg, Table of Isotopes, Revs. Modern Phys. 30, 585 (1958).

16. J. F. Eichelberger, K. C. Jordan, S. R. Orr, and J. R. Parks, Phys. Rev. 96, 719 (1954).

17. W. John, Jr., Phys. Rev. 103, 704 (1956).

18. C. G. Andre, J. R. Huizinga, J. F. Mech, W. J. Ramler, E.G. Rauh, and S. R. Rocklin, Phys. Rev. 101, 645 (1956).

19. This Q value was calculated from the atomic masses tabulated in A. G. W. Cameron, A Revised Semi-Empirical Atomic Mass Formula (with Appended Table of Mass Excesses and Nuclear Reaction Energies), Atomic Energy of Canada, Ltd., Chalk River Project Report CRP-690, 1957 (unpublished).

20. J. O. Rasmussen, Jr., S. G. Thompson, and A. Ghiorso, Phys. Rev. 89, 33 (1953).

21. This Q value was calculated from the tabulation of Ref. 19. Measured values are available for calculating the Q's up to the (C^{12}, 4n) reaction for this system.[22] Q's up to (C^{12}, 4n) calculated from both sets of values agree to within 1.0 Mev.

22. A. Wapstra, in Handbuch der Physik, Vol. 38 (Springer-Verlag, Berlin, 1958), p. 1.

23. W. F. Baldridge and D. N. Hume, in Radiochemical Studies: The Fission Products, Book 3, C. D. Coryell and N. Sugarman, Eds. (McGraw-Hill Book Co., New York, 1951), paper 294.

24. B. P. Bayhurst and R. J. Prestwood, Nucleonics 17, No. 3, 82 (1959).

25. H. Marshall Blann, Fission of Gold with 112-Mev C^{12} Ions: a Mass-Yield and Charge-Distribution Study (Ph. D. Thesis), Lawrence Radiation Laboratory Report, UCRL-9190, May 1960 (unpublished), Fig. 23.

26. A. R. Brosi and B. H. Ketelle, Phys. Rev. 100, 169 (1955).

27. J. Chubbock and I. Perlman, Phys. Rev. 74, 982 (1948).

28. R. D. Hill, Phys. Rev. 82, 449 (1951).

29. H. B. Keller and J. M. Cork, Phys. Rev. 84, 1079 (1951).

30. G. P. Milburn and L. Schecter, Graphs of RMS Multiple-Scattering Angle and Range Straggling for High-Energy Charged Particles, University of California Radiation Laboratory Report UCRL-2234, January 1954 (unpublished).

31. B. G. Harvey and W. H. Wade, Lawrence Radiation Laboratory, Berkeley (unpublished data).

32. Johnson, Matthey and Co., London, spectroscopically analyzed chemicals.

33. Baker Analyzed Reagent lead pellets. Impurities: Ag 5×10^{-5}%, Bi 10^{-4}%, Fe 10^{-3}%; J. T. Baker Chemical Co., Phillipsburg, N. J.

34. Alfred Chetham-Strode, Jr., Light Isotopes of Berkelium and Californium (Ph. D. Thesis), University of California Radiation Laboratory Report UCRL-3322, June 26, 1956 (unpublished).

35. Richard W. Hoff, Orbital Electron Capture in the Heaviest Elements (Ph. D. Thesis), University of California Radiation Laboratory Report UCRL-2325, September 1953 (unpublished).

36. G. W. Barton, Jr., A. Ghiorso, and I. Perlman, Phys. Rev. 82, 13 (1951).

37. P. R. Gray, Phys. Rev. 101, 1306 (1956).

38. S. Ulam and J. von Neumann, Bull. Am. Math. Soc. 53, 1120 (1947).

39. M. L. Goldberger, Phys. Rev. 74, 1269 (1948).

40. G. Bernardini, E. T. Booth, and S. J. Lindenbaum, Phys. Rev. 88, 1017 (1952).

41. G. C. Morrison, H. Muirhead, and W. G. V. Rosser, Phil. Mag. 44, 1326 (1953).

42. H. McManus, W. T. Sharp, and H. Gellmann, Phys. Rev. 93, 924 (1954).

43. P. Cüer and J. Combe, Compt. rend. 238, 1799 (1954).

44. J. W. Meadows, Phys. Rev. 98, 744 (1955).

45. P. Cüer and J. Combe, J. phys. radium 16, 295 (1955).

46. J. Combe, Nuovo cimento 3, S-182 (1956).

47. Gösta Rudstam, Spallation on Medium-Weight Elements (Ph. D. Thesis), Gustav Werner Institute for Nuclear Chemistry, University of Uppsala, 1956 (unpublished).

48. N. S. Ivanova and I. I. Pianov, JETP 4, 367 (1957).

49. N. Metropolis et al., Phys. Rev. 110, 185 (1958).

50. N. Metropolis et al., Phys. Rev. 110, 204 (1958).

51. N. N. Chavchanidze, Izvest. Akad. Nauk S.S.S.R. Ser. Fiz. 19, 629 (1955).

52. I. Dostrovsky, P. Rabinowitz, and R. Bivins, Phys. Rev. 111, 1659 (1958).

53. J. D. Jackson, Can. J. Phys. 35, 21 (1957).

54. I. Dostrovsky, Z. Fraenkel, and P. Rabinowitz, Proceedings of the Second United Nations International Conference on the Peaceful Uses of Atomic Energy, Vol. 15 (United Nations, Geneva, 1958), p. 301.

55. I. Dostrovsky, Z. Fraenkel, and G. Friedlander, Phys. Rev. 116, 683 (1959).

56. I. Dostrovsky, Z. Fraenkel, and L. Winsberg, Phys. Rev. 118, 781 (1960).

57. N. Bohr, Nature 137, 344 (1936).

58. V. F. Weisskopf, Phys. Rev. 52, 295 (1937).

59. V. F. Weisskopf, and D. H. Ewing, Phys. Rev. 57, 472 (1940).

60. J. D. Jackson, Can. J. Phys. 34, 767 (1956).

61. Programmer's Primer for FORTRAN Automatic Coding System for the IBM 704 Data Processing System (International Business Machines Corp., New York, 1957), Form No. 32-0306-1.

62. Reference Manual FORTRAN Automatic Coding System for the IBM 704 Data Processing System (International Business Machines Corp., New York, 1959), Form No. 28-6003-1.

63. T. Ericson and V. Strutinski, Nuclear Phys. 8, 284 (1958); with corrections from Nuclear Phys. 9, 689 (1959).

64. I. Halpern and V. Strutinski, Proceedings of the Second United Nations International Conference on the Peaceful Uses of Atomic Energy, Vol. 15 (United Nations, Geneva, 1958).

65. G. A. Pik-Pichak, Soviet Physics JETP 11, 557 (1960); J. Exptl. Theoret. Phys. (USSR) 38, 768 (1960).

66. K. J. Le Couteur, Nuclear Reactions, Vol. 1, P. M. Endt and M. Demeur, Eds. (North-Holland Publishing Co., Amsterdam, 1959).

67. K. J. Le Couteur and D. W. Lang, Nuclear Phys. 13, 32, (1959).

68. D. W. Lang and K. J. Le Couteur, Proc. Phys. Soc. (London) 67A, 585 (1954).

69. The angles given here are determined by the mean radii of the catcher foil rings and a 4.0 cm target-to-catcher distance. The angular increments intercepted by the successive rings are: 4.64, 2.66, 2.82, 2.70, 2.88, 2.42, 2.56, 2.40, 2.38, 2.26, and 2.10 degrees. These increments correspond to spherical zones of relative area: 1.00, 1.48, 2.29, 2.81, 3.79, 3.76, 4.56, 4.77, 5.20, 5.38, and 5.68.

70. The angles given here are determined by the mean radii of the catcher foil rings and 6.0 cm target-to-catcher distance. The angular increments intercepted by the successive rings are: 3.08, 1.80, 1.90, 1.84, 1.96, 1.68, 1.92, 1.76, 1.72, 1.70, and 1.60 degrees. These increments correspond to spherical zones of relative area: 1.00, 1.47, 2.22, 2.84, 3.95, 3.94, 4.83, 5.37, 5.75, 6.29, and 6.45.

71. J. M. Alexander and L. Winsberg, Phys. Rev. 121, 529 (1961).

72. K. O. Nielsen, Electromagnetically Enriched Isotopes and Mass Spectometry (Butterworth and Co., London, 1956).

73. L. Winsberg and J. M. Alexander, Phys. Rev. 121, 518 (1961).

74. N. Bohr, Kgl. Danske Videnskab. Selskab, Mat.-fys. Medd. 18, No. 8 (1948).

75. J. Lindhard and M. Scharff, as quoted in R. B. Leachman and H. Atterling, Arkiv Fysik 13, 101 (1957).

76. E. B. Mode, The Elements of Statistics (Prentice-Hall, Inc., New York, 1941).

77. J. M. Alexander, Lawrence Radiation Laboratory, Berkeley (unpublished data).

78. R. Vandenbosch and G. T. Seaborg, Phys. Rev. 110, 507 (1958).

79. A. G. W. Cameron, Can. J. Phys. 36, 1040 (1958).

80. Ernest W. Valyoscik, Range and Range Straggling of Heavy Recoil Atoms (M.S. Thesis), Lawrence Radiation Laboratory Report UCRL-8855, November 1959 (unpublished).

81. Bernard G. Harvey, Lawrence Radiation Laboratory, Berkeley (unpublished calculations--see Ref. 80).

82. H. W. Broek, Neutron Emission from Compound Systems of High Angular Momentum (Ph.D. Thesis), Yale University, 1960 (unpublished).

83. W. J. Knox, Proceedings of the Second Conference on Reactions Between Complex Nuclei (John Wiley and Sons, New York, 1960).

84. J. R. Huizinga, Argonne National Laboratory, Lemont, Ill. (private communication).

85. C. Bloch, Phys. Rev. 93, 1094 (1954).

86. G. R. Satchler, Proceedings of the Conference on Reactions Between Complex Nuclei (Gatlinburg), Oak Ridge National Laboratory Report ORNL-2606, 1958 (unpublished).

87. T. Ericson, Nuclear Phys. 11, 481 (1959).

88. T. Ericson, Nuclear Phys. 17, 250 (1960).

89. A. C. Douglas and N. MacDonald, Nuclear Phys. 13, 389 (1959).

90. T. Kammuri and R. Nakasima, Proceedings of the Second Conference on Reactions Between Complex Nuclei (Gatlinburg), John Wiley and Sons, Inc., New York, 1960.

91. A. S. Karamyan, Y. B. Gerlit, and B. R. Myasoedov, JETP 9, 431 (1959); J. Exptl. Theoret. Phys. (USSR) 36, 621 (1959).

92. Glen E. Gordon, Fission and Spallation in Nuclear Reactions Induced by Heavy Ions (Ph. D. Thesis), Lawrence Radiation Laboratory Report, UCRL-9083, May 1960 (unpublished).

93. B. R. Mottelson and J. G. Valatin, Phys. Rev. Letters 5, 511 (1960).

94. T. D. Thomas, Proceedings of the Second Conference on Reactions Between Complex Nuclei (Gatlinburg), John Wiley and Sons, New York, 1960. See remarks following Paper D-4.

95. T. D. Thomas, Phys. Rev. 116, 703 (1959).

96. G. Brown and H. Muirhead, Phil. Mag. 2, 473 (1957).

97. L. Rosen and L. Stewart, Phys. Rev. 107, 824 (1957).

98. D. C. Peaslee, Annual Reviews of Nuclear Science, Vol. 5, E. Segrè, Ed (Annual Reviews, Inc., Palo Alto, Calif., 1955), p. 99.

99. H. H. Barschall, C. K. Bockelman, R. E. Peterson, and R. K. Adair, Phys. Rev. 76, 1146 (1949).

100. J. M. Blatt and V. F. Weisskopf, Theoretical Nuclear Physics (John Wiley and Sons, New York, 1952), pg. 773.

101. R. Serber, Phys. Rev. 72, 1008 (1947).

102. Robert J. Silva, Mechanisms of the (α,pn) Reaction (Ph. D. Thesis), Lawrence Radiation Laboratory Report UCRL-8678, March 1959 (unpublished).

This report was prepared as an account of Government sponsored work. Neither the United States, nor the Commission, nor any person acting on behalf of the Commission:

A. Makes any warranty or representation, expressed or implied, with respect to the accuracy, completeness, or usefulness of the information contained in this report, or that the use of any information, apparatus, method, or process disclosed in this report may not infringe privately owned rights; or

B. Assumes any liabilities with respect to the use of, or for damages resulting from the use of any information, apparatus, method, or process disclosed in this report.

As used in the above, "person acting on behalf of the Commission" includes any employee or contractor of the Commission, or employee of such contractor, to the extent that such employee or contractor of the Commission, or employee of such contractor prepares, disseminates, or provides access to, any information pursuant to his employment or contract with the Commission, or his employment with such contractor.